22-45-48

VI-B-37

THERMAL STRATIFICATION AND CIRCULATION OF WATER BODIES SUBJECTED TO THERMAL DISCHARGE

A. N. Nahavandi and M. A. Borhani
New Jersey Institute of Technology
Newark, New Jersey U.S.A.

ABSTRACT

A three-dimensional analytical model for large water bodies is presented. Time histories and spatial distribution of pressure, velocity and temperature in water bodies, subjected to thermal discharge, are determined employing a digital computer. The dynamic response is obtained for a rectangular water body by applying a finite difference method to the mass, momentum, and energy balance equations. The distinctive feature of this analysis, as compared to previous studies, is the calculation of pressure and water level from equations of motion without simplifying assumptions such as hydrostatic pressure approximation and rigid-lid concept. The mathematical formulation is verified by applying this analysis to cases where the final steady state flow patterns have been determined analytically or experimentally by others. The problem of thermal discharge entering a river is then analyzed. The time histories of the velocity and temperature distribution are obtained. These results provide the values of temperature rise and the rate of temperature rise needed for the assessment of thermal pollution in water bodies.

INTRODUCTION

Thermal power and industrial processing plants use large quantities of cooling water from natural or artificial water bodies and return the water to the source at higher temperatures. When the thermal discharge from a plant, into a water body, raises the water temperature by such an extent as to damage aquatic life or other legitimate uses of the water source, some degree of thermal pollution exists.

To assess the extent of a thermal pollution, utilities, ecologists, federal and state agencies as well as the public are interested in determining the space and time distribution of temperature within a water body, when it is subjected to a prescribed thermal load.

The theoretical analysis of the dynamic behavior of a large water body, subjected to thermal discharge, is based on the solution of space- and time-dependent conservation and state equations. Conservation of mass, momentum, and energy for the water flow in the impoundment together with the equation of state, provide a sufficient number of partial differential equations and algebraic relations in space and time for the solution

of the problem. Although, these equations have been known for over a century, due to their highly nonlinear nature, a direct closed form analytical solution is considered practically impossible for most general cases involving realistic geometries and boundary conditions. The available mathematical solutions of problems involving thermal discharge are severely limited by the many simplifying assumptions made in order to achieve a solution. In fact, analytical solutions to the problems of thermal discharge are obtained only for problems involving simple geometry and boundary conditions. Solutions to more realistic geometries and boundary conditions can be sought only by the development of computer modeling in three-dimensions under transient conditions.

Current three-dimensional computer simulation of thermal discharge into water bodies are based on a number of simplifying assumptions discussed hereunder:

1. Compliance with the Conservation of Mass and Momentum

Generally, the three components of water velocity are found from the longitudinal, lateral, and vertical momentum equations. These three components of velocity should satisfy the conservation of mass equation. A major difficulty arises when simultaneous compliance with the principles of conservation of mass and momentum cannot be ensured. Under the Boussinesq approximation, the conservation of mass reduces to zero divergence for the water velocity (with no mass storage term) i.e. the sum of all inflows to and outflows from any fluid control volume in the flow field must vanish. Since the new velocity components, calculated by the integrations of the momentum equations do not necessarily satisfy the continuity equation, the mass balance would be disturbed, thereby yielding a small surplus or deficit inflow at certain control volumes. To resolve this dilemma, Brady and Geyer [1] hypothesize that the surplus or deficit inflows redistribute in all directions by equal magnitude. Obviously, the disadvantage of this velocity adjustment technique is that the adjusted velocities no longer satisfy the momentum equations. Considering a water body, such as a river, flowing longitudinally with a laterally uniform velocity distribution, and applying the appropriate boundary conditions on the lateral velocities at the thermal discharge location, they found that the out-of-balance surplus inflow to each adjacent cell is exceptionally large. When their model attempts to distribute this surplus inflow among the surrounding fluid cells, the resulting vertical velocity adjustment becomes excessively large which aborts the run. Brady and Geyer, referred to this problem as the "vertical overresponsiveness of the model" and devised schemes to suppress the associated undesirable vertical fluctuations by either: 1) temporarily suppressing vertical redistribution such that each fluid layer achieves its own mass balance independently; or 2) temporarily enforcing a rigid lid at the fluid free surface such that a zero vertical velocity is maintained at the most upper layer of the model at every fluid cell. The rigid lid assumption is used by many authors to simplify the solution to

the stratification and circulation in water bodies [2, 3, 4]. Obviously, this situation calls for an improved approach for a simultaneous compliance with the conservation equations of mass and momentum.

2. Surface Flow Distribution

The treatment of the slope variation at the water free surface constitutes another major difficulty. The upwelling (or downwelling) flow at the surface creates positive (or negative) surge waves [5, 6]. The mathematical modeling of these phenomena under unsteady flow conditions is complicated. To resolve this difficulty Waldrop and Farmer [7] first assumed that the vertical component of velocity near the surface will be redirected in the horizontal direction (in x and y directions) and the surface will move. Later Waldrop and Farmer [8] in a major effort to resolve the surface flow distribution problem introduced a mass balance at the free surface and extended their horizontal momentum equations to elements near the water surface. This situation calls for further studies of the behavior of the free surface under unsteady flow conditions.

3. Pressure Distribution

The velocity components in the flow field are extremely sensitive to values of nodal pressures. Slight changes in the pressure distribution would affect the circulation in the water body considerably. The calculation of the correct pressure distribution is, therefore, of paramount importance. Most authors [9, 10, 11, 12, 13, 14, 15] assume that the total dynamic pressure at each point in the flow is equal to hydrostatic pressure obtained under static conditions. This assumption, referred to as hydrostatic approximation, leads to inaccuracies in regions of severe upwelling and downwelling which will adversely affect the correctness of circulation velocities. Thus, a better technique for the computation of the pressure field is called for.

4. Numerical Stability

Calculations of space and time increments for obtaining a stable numerical solution of partial differential equations of mass, momentum and energy conservation is a difficult task. Most authors resort to overly simplified criteria for the establishment of the upper bound of the integration time step for an assumed set of space increments. Brady and Geyer [1] state that the maximum integration step appears to be limited by relationships between the velocities and the smallest cell dimensions in each direction. Waldrop and Farmer [7], and Harlow and Welch [16] resort to a stability limit calculated on the basis of one-dimensional, unsteady incompressible flow equations with a free surface. This limit imposes an upper bound on their integration time step equal to the ratio of the smallest cell size and the surface wave speed. More accurate means for the prediction of the space and time increments are needed.

Most authors believe that much work is still required to refine various

features of the present unsteady three-dimensional computer models before the present models can be applied to situations involving significant stratification effects, or fluctuations in flow in water bodies.

The main objectives of the present study are as follows:

1) To develop an improved three-dimensional analytical model for the mathematical description of a large rectangular water body subjected to a thermal discharge.

2) To develop a numerical integration technique for solving the above mathematical model on a digital computer.

3) To develop a digital computer program for predicting the thermal stratification and circulation phenomena in a given rectangular water body subjected to thermal discharge and to determine the time histories and spatial distribution of pressure, velocity and temperature fields within the water body.

The major contribution and distinctive features of the present study, as compared with the previous works in this general area, can be summarized as follows:

A) Compliance with the conservation of mass and momentum is obtained by the introduction of two flow regions in the entire flow field: a) the water-level region containing a portion of water near the free surface in which the water level rises or falls, as the case may be,during the dynamic solution; and b) the sub-water-level region located under the water level region which remains totally filled with fluid at all times during the transient. As will be seen later, the superimposition of a three-dimensional grid on these two regions facilitates the simultaneous compliance with the principles of conservation of mass and momentum for the entire flow field without any mass imbalance.

B) A different set of differential equations for the conservation of mass, momentum and energy is applied to the cells located in the water-level and sub-water-level flow regions. This is necessary because the cells in the sub-water-level region have a variable height while the cells in the sub-water-level region have a constant height.

C) The pressure distribution is obtained by combining the momentum and continuity equations. This feature eliminates the need for the hydrostatic pressure approximation.

D) A detailed numerical stability analysis is performed which provides accurate criteria for the selection of the space and time increments.

MATHEMATICAL FORMULATION

Simplifying Assumptions

The mathematical formulation in this study is based on the following assumptions:

1) The equations of motion, energy and continuity are applied in their time-smoothed form to turbulent incompressible three-dimensional flow with Cartesian coordinates, as shown in Figure 1, with z positive upward.

2) It is assumed that Boussinesq's approximation applies. In other words, densities are treated as constants except in terms involving gravity. This allows natural circulation to take place. Furthermore, density in the body force term is considered to be a function of temperature only.

3) The effects of turbulence are modeled by using eddy transport coefficients. Horizontal and vertical momentum eddy viscosities and thermal eddy diffusivities are considered as constants throughout the body of water though different magnitudes for horizontal and vertical directions.

4) It is assumed that there are no internal heat sources and the heat exchange between the water body and the atmosphere takes place near the water free surface.

5) Loss of mass due to evporation at the surface and conductive heat transfer through the impoundment solid boundaries are generally small and are neglected.

6) The Coriolis forces acting on the water body is considered to be negligible.

The boundary conditions of the problem involve: 1) the geometry of the impoundment including the thermal discharge inlet, as well as the river inflows and outflows configurations; 2) the mass flow rates of the inflows across the boundaries; and 3) the level, pressure and temperature along the inlet boundaries. It is assumed that all of the above parameters are known.

The initial conditions of the problem includes the pressure, velocity, level and temperature distributions of the impoundment at time t = 0. These variables are computed by the present program by first performing a dynamic analysis under no thermal discharge conditions and then using the calculated pressure, velocity, level and temperature distributions, as initial conditions, in a dynamic analysis involving a thermal discharge.

Governing Equations

The mathematical formulation of the sub-water-level flow region consists of the following fundamental equations [17].

Momentum equations:

$$\frac{\partial u}{\partial t} + u\frac{\partial u}{\partial x} + v\frac{\partial u}{\partial y} + w\frac{\partial u}{\partial z} = -\frac{1}{\rho_0}\frac{\partial p}{\partial x} + \nu_h\left(\frac{\partial^2 u}{\partial x^2} + \frac{\partial^2 u}{\partial y^2}\right) + \nu_v\frac{\partial^2 u}{\partial z^2} \tag{1}$$

$$\frac{\partial v}{\partial t} + u\frac{\partial v}{\partial x} + v\frac{\partial v}{\partial y} + w\frac{\partial v}{\partial z} = -\frac{1}{\rho_0}\frac{\partial p}{\partial y} + \nu_h\left(\frac{\partial^2 v}{\partial x^2} + \frac{\partial^2 v}{\partial y^2}\right) + \nu_v\frac{\partial^2 v}{\partial z^2} \tag{2}$$

$$\frac{\partial w}{\partial t} + u\frac{\partial w}{\partial x} + v\frac{\partial w}{\partial x} + w\frac{\partial w}{\partial z} = -\frac{1}{\rho_0}\frac{\partial p}{\partial z} + \nu_h\left(\frac{\partial^2 w}{\partial x^2} + \frac{\partial^2 w}{\partial y^2}\right) + \nu_v\frac{\partial^2 w}{\partial z^2} - g\frac{\rho}{\rho_0} \tag{3}$$

Continuity equation:

$$\frac{\partial u}{\partial x} + \frac{\partial v}{\partial y} + \frac{\partial w}{\partial z} = 0 \tag{4}$$

Energy equation:

$$\frac{\partial T}{\partial t} + u\frac{\partial T}{\partial x} + v\frac{\partial T}{\partial y} + w\frac{\partial T}{\partial z} = D_h\left(\frac{\partial^2 T}{\partial x^2} + \frac{\partial^2 T}{\partial y^2}\right) + D_v\frac{\partial^2 T}{\partial z^2} \tag{5}$$

Equation of state:

$$\rho = \rho\ (T) \tag{6}$$

In this study, the thermal discharge parameters are used as reference values for the non-dimensionalization of the governing equations. Let U_0, ρ_0, T_0 and d_0 be the velocity, density, temperature and half width of thermal discharge flow respectively. The dimensionless quantities are defined by

$$x^* = \frac{x}{d_0} \qquad y^* = \frac{y}{d_0} \qquad z^* = \frac{z}{d_0} \tag{7}$$

$$u^* = \frac{u}{U_0} \qquad v^* = \frac{v}{U_0} \qquad w^* = \frac{w}{U_0} \tag{8}$$

$$t^* = \frac{tU_0}{d_0} \qquad T^* = \frac{T}{T_0} \qquad p^* = \frac{p}{\rho_0 g d_0} \tag{9}$$

$$\rho^* = \frac{\rho}{\rho_0} \tag{10}$$

Employing the above dimensionless variables in the continuity, momentum and energy equations, one obtains the time derivatives for velocity components u, v, w and temperature T in parabolic differential form as follows:

$$\frac{\partial u^*}{\partial t^*} = - u^* \frac{\partial u^*}{\partial x^*} - v^* \frac{\partial u^*}{\partial y^*} - w^* \frac{\partial u^*}{\partial z^*} - \frac{1}{F_0^2} \frac{\partial p^*}{\partial x^*}$$
$$+ \frac{\nu_h}{\nu_0} \frac{1}{R_0} \left(\frac{\partial^2 u^*}{\partial x^{*2}} + \frac{\partial^2 u^*}{\partial y^{*2}}\right) + \frac{\nu_v}{\nu_0} \frac{1}{R_0} \frac{\partial^2 u^*}{\partial z^{*2}} \tag{11}$$

$$\frac{\partial v^*}{\partial t^*} = - u^* \frac{\partial v^*}{\partial x^*} - v^* \frac{\partial v^*}{\partial y^*} - w^* \frac{\partial v^*}{\partial z^*} - \frac{1}{F_0^2} \frac{\partial p^*}{\partial y^*}$$
$$+ \frac{\nu_h}{\nu_0} \frac{1}{R_0} \left(\frac{\partial^2 v^*}{\partial x^{*2}} + \frac{\partial^2 v^*}{\partial y^{*2}}\right) + \frac{\nu_v}{\nu_0} \frac{1}{R_0} \frac{\partial^2 v^*}{\partial z^{*2}} \tag{12}$$

$$\frac{\partial w^*}{\partial t^*} = u^* \frac{\partial w^*}{\partial x^*} - v^* \frac{\partial w^*}{\partial y^*} - w^* \frac{\partial w^*}{\partial z^*} - \frac{1}{F_0^2} \frac{\partial p^*}{\partial z^*} - \frac{\rho^*}{F_0^2}$$
$$+ \frac{\nu_h}{\nu_0} \frac{1}{R_0} \left(\frac{\partial^2 w^*}{\partial x^{*2}} + \frac{\partial^2 w^*}{\partial y^{*2}}\right) + \frac{\nu_v}{\nu_o} \frac{1}{R_0} \frac{\partial^2 w^*}{\partial z^{*2}} \tag{13}$$

$$\frac{\partial T^*}{\partial t^*} = - u^* \frac{\partial T^*}{\partial x^*} - v^* \frac{\partial T^*}{\partial y^*} - w^* \frac{\partial T^*}{\partial z^*}$$
$$+ \frac{D_h}{\nu_0} \frac{1}{R_0} \left(\frac{\partial^2 T^*}{\partial x^{*2}} + \frac{\partial^2 T^*}{\partial y^{*2}}\right) + \frac{D_v}{\nu_0} \frac{\partial^2 T^*}{\partial z^{*2}} \tag{14}$$

with continuity and state equations given by

$$\frac{\partial u^*}{\partial x^*} + \frac{\partial v^*}{\partial y^*} + \frac{\partial w^*}{\partial z^*} = 0 \tag{15}$$

$$\rho^* = \rho^* (T^*) \tag{16}$$

In the above equations, the following dimensionless numbers are used

1) Froude number $F_0 = U_0/(gd_0)^{1/2}$ (17)

2) Reynolds number $R_0 = U_0 d_0/\nu_0$ (18)

Equations (11) to (16) are a set of six equations that will be used for the determination of six unknowns, u*, v*, w*, p*, ρ* and T* as functions of time and space.

The final equations, including the pressure equation, are obtained from

the above equations as follows. First, the continuity equation is differentiated with respect to time to give

$$\frac{\partial}{\partial t^*}\left(\frac{\partial u^*}{\partial x^*} + \frac{\partial v^*}{\partial y^*} + \frac{w^*}{\partial z^*}\right) = 0 \tag{19}$$

The order of differentiation in equation (19) is then interchanged

$$\frac{\partial}{\partial x^*}\left(\frac{\partial u^*}{\partial t^*}\right) + \frac{\partial}{\partial y^*}\left(\frac{\partial v^*}{\partial t^*}\right) + \frac{\partial}{\partial z^*}\left(\frac{\partial w^*}{\partial t^*}\right) = 0 \tag{20}$$

To facilitate spatial differentiations indicated by eq. (20), eq. (11) through (13) are first rewritten in the following form

$$\frac{\partial u^*}{\partial t^*} = Q_y^* - \frac{1}{F_0^2}\frac{\partial p^*}{\partial x^*} \tag{21}$$

$$\frac{\partial v^*}{\partial t^*} = Q_y^* - \frac{1}{F_0^2}\frac{\partial p^*}{\partial y^*} \tag{22}$$

$$\frac{\partial w^*}{\partial t^*} = Q_z^* - \frac{1}{F_0^2}\frac{\partial p^*}{\partial z^*} \tag{23}$$

where

$$Q_x^* = -u^*\frac{\partial u^*}{\partial x^*} - v^*\frac{\partial u^*}{\partial y^*} - w^*\frac{\partial u^*}{\partial z^*} + \frac{\nu_h}{\nu_0}\frac{1}{R_0}\left(\frac{\partial^2 u^*}{\partial x^{*2}} + \frac{\partial^2 u^*}{\partial y^{*2}}\right) + \frac{\nu_v}{\nu_0}\frac{1}{R_0}\frac{\partial^2 u^*}{\partial z^{*2}} \tag{24}$$

$$Q_y^* = -u^*\frac{\partial v^*}{\partial x^*} - v^*\frac{\partial v^*}{\partial y^*} - w^*\frac{\partial v^*}{\partial z^*} + \frac{\nu_h}{\nu_0}\frac{1}{R_0}\left(\frac{\partial^2 v^*}{\partial x^{*2}} + \frac{\partial^2 v^*}{\partial y^{*2}}\right) + \frac{\nu_v}{\nu_0}\frac{1}{R_0}\frac{\partial^2 v^*}{\partial z^{*2}} \tag{25}$$

$$Q_z^* = -u^*\frac{\partial w^*}{\partial x^*} - v^*\frac{\partial w^*}{\partial y^*} - w^*\frac{\partial w^*}{\partial z^*} + \frac{\nu_h}{\nu_0}\frac{1}{R_0}\left(\frac{\partial^2 w^*}{\partial x^{*2}} + \frac{\partial^2 w^*}{\partial y^{*2}}\right) + \frac{\nu_v}{\nu_0}\frac{1}{R_0}\frac{\partial^2 w^*}{\partial z^{*2}} - \frac{\rho^*}{F_0^2} \tag{26}$$

with

$$\frac{\partial w^*}{\partial z^*} = -\left(\frac{\partial u^*}{\partial x^*} + \frac{\partial v^*}{\partial z^*}\right) \tag{27}$$

substituting eqs. (21) through (23) into (20) yields

$$\nabla^2 p^* = F_0^2 \left(\frac{\partial Q_x^*}{\partial x^*} + \frac{\partial Q_y^*}{\partial y^*} + \frac{\partial Q_z^*}{\partial z^*}\right) \tag{28}$$

This elliptic differential equation will provide a means for the calculation of the pressure distribution in the water body. Eqs. (27), (24), (25), (26), (28), (21), (22), (14) and (16) constitute our final equations which will be solved for updated values of w^*, Q_x^*, Q_y^*, Q_z^*, p^*, u^*, v^*, T^*, and ρ^* respectively. It should be noted that: The vertical momentum equation (23) is used indirectly in this computation through its usage in the derivation of the pressure equation (28). Since the water level variation provides a vertical freedom for the water body, it is imperative to calculate the vertical velocity component w^* from the continuity equation and not by the application of the momentum equation in the vertical direction equation (23). However, the momentum balance in the vertical direction is fully satisfied since eq. (23) is explicitly used in the derivation of the pressure equation (28). In fact, eq. (23) may be easily derived from the final equation stated above.

The mathematical formulation for the water-level flow region is derived by the application of the fundamental equations of mass, momentum and energy as follows. The water level in cells located at the air-water interface varies with time and space. For this reason, the continuity equation, as given by eq. (27), is not valid for these cells. Application of a mass balance to such a cell with all sides fixed in space except the top which moves with the water level, yields

$$\begin{aligned}\frac{\partial}{\partial t}(\rho \Delta x \Delta y\, H) = {} & (\rho u \Delta y\, H)_x - (\rho u \Delta y\, H)_{x+\Delta x} \\ & + (\rho v \Delta x\, H)_y - (\rho v \Delta x\, H)_{y+\Delta y} \\ & + (\rho w \Delta x \Delta y)_z - (\rho w \Delta x \Delta y)_{z+H}\end{aligned} \tag{29}$$

The last term represents the mass flux leaving the water level surface. Since the evaporation losses are considered insignificant, this term is equal to zero. Dividing both sides of the above equation by $\rho \Delta x \Delta y$, considering ρ to be constant and equat to ρ_0 consistent with Boussinesq approximation used earlier, letting Δx, Δy approach zero and using dimensionless variables yields

$$\frac{\partial H^*}{\partial t^*} = -\frac{\partial}{\partial x^*}(u^* H^*) - \frac{\partial}{\partial y^*}(v^* H^*) + w^* \tag{30}$$

where

$$H^* = \frac{H}{d_0} \tag{31}$$

Similarly, application of the energy and momentum balance to the water-level region gives:

$$\frac{\partial T^*}{\partial t^*} = - u^* \frac{\partial T^*}{\partial x^*} - v^* \frac{\partial T^*}{\partial y^*} + \frac{D_h}{\nu_0} \frac{1}{R_0 H^*} \left[\frac{\partial}{\partial x^*} \left(H^* \frac{\partial T^*}{\partial x^*}\right)\right.$$
$$\left. + \frac{\partial}{\partial y^*} \left(H^* \frac{\partial T^*}{\partial y^*}\right)\right] - \frac{D_v}{\nu_0} \frac{1}{R_0 H^*} \frac{\partial T^*}{\partial z^*} - \frac{S_0}{H^*} (T^* - E^*) \tag{32}$$

$$\frac{\partial u^*}{\partial t^*} = - u^* \frac{\partial u^*}{\partial x^*} - v \frac{\partial u^*}{\partial y^*} - \frac{1}{F_0^2 H^*} \frac{\partial H^* p^*}{\partial x^*}$$
$$+ \frac{\nu_h}{\nu_0} \frac{1}{R_0 H^*} \left[\frac{\partial}{\partial x^*} \left(H^* \frac{\partial u^*}{\partial x^*}\right) + \frac{\partial}{\partial y^*} \left(H^* \frac{\partial u^*}{\partial y^*}\right)\right]$$
$$- \frac{\nu_v}{\nu_0} \frac{1}{R_0 H^*} \frac{\partial u^*}{\partial z^*} + \frac{1}{2} \frac{C_{fx} \rho_a^* W_x^{*2}}{H^*} \tag{33}$$

$$\frac{\partial v^*}{\partial t^*} = - u^* \frac{\partial v^*}{\partial x^*} - v^* \frac{\partial v^*}{\partial y^*} - \frac{1}{F_0^2 H^*} \frac{\partial H^* p^*}{\partial y^*}$$
$$+ \frac{\nu_h}{\nu_0} \frac{1}{R_0 H^*} \left[\frac{\partial}{\partial x^*} \left(H^* \frac{\partial v^*}{\partial x^*}\right) + \frac{\partial}{\partial y^*} \left(H^* \frac{\partial v^*}{\partial y^*}\right)\right]$$
$$- \frac{\nu_v}{\nu_0} \frac{1}{R_0 H^*} \frac{\partial v^*}{\partial z^*} + \frac{1}{2} \frac{C_{fy} \rho_a^* W_y^{*2}}{H^*} \tag{34}$$

Where S_0, the Stanton number, is defined by

$$S_0 = \frac{K}{\rho_0 C_p U_0} \tag{35}$$

and

$$\rho_a^* = \frac{\rho_a}{\rho_0} \tag{36}$$

$$W_x^* = \frac{W_x}{U_0} \qquad W_y^* = \frac{W_y}{U_0} \tag{37}$$

The pressure at the air-water interface is always atmospheric and can be considered equal to zero no matter what the water level may be at any instant of time. For this reason, the pressure at the center of the water level can be considered to be hydrostatic, i.e. for the water level element

$$p^* = \rho^* H^* \tag{38}$$

This equation may also be derived by applying a momentum balance, in the vertical direction, in the water-level flow region and noting that the water vertical velocity in this region is relatively small and therefore negligible. The pressure distribution given by eq. (38) is substituted into the horizontal momentum equations.

It is important to realize the difference between the flow patterns in the flow field and the water level elements. In the flow field elements, an increase in the fluid boundary velocity, will induce horizontal velocity components. However, the time constant associated with the momentum equations will not permit these equations to respond instantaneously to the boundary velocity disturbance at the river or thermal discharge inlets. Because of the flow incompressibility and since the fluid vertical inertia is considerably smaller than the horizontal inertias, the mass imbalance will result in a positive vertical fluid motion designated as "upwelling". This vertical motion will continue upward until it reaches the water level element where by virtue of eq. (30) will cause the water level to rise. This rise is large for elements close to the boundary disturbance and small for elements farther away. This spatial change affects the horizontal momentum equation (33) and (34) and induce a horizontal flow in the water level elements which in turn tends to reduce the water level through eq. (30). A reverse situation takes place when the boundary velocity is decreased. The mass imbalance will result in a negative fluid motion, designated as "downwelling". This will cause the lowering of the water level with an attendant horizontal flow into the element to increase the water level.

Boundary Conditions

The water body boundary surfaces may be classified as follows:

Type (1): The surface boundary located at the water level free surface.

Type (2): The lateral solid-fluid boundary located at the interface between the impoundment wall and the water body.

Type (3): The bottom boundary located at the bottom of the impoundment.

Type (4): The fluid-fluid boundary located at the interface between the water body in the region of interest and surrounding waters.

For the surface boundary, the pressure is considered atmospheric at the

air-water interface and is set equal to zero. For the lateral solid-fluid and bottom boundaries, application of the momentum equation in the direction normal to the boundaries gives the following equation respectively

$$\frac{\partial p^*}{\partial y^*} = F_0^2 \frac{\nu_h}{\nu_0} \frac{1}{R_0} \frac{\partial^2 v^*}{\partial y^{*2}} \tag{39}$$

$$\frac{\partial p^*}{\partial z^*} = -\rho^* + F_0^2 \frac{\nu_v}{\nu_0} \frac{1}{R_0} \frac{\partial^2 w^*}{\partial z^{*2}} \tag{40}$$

For the fluid-fluid boundaries, the pressure distribution at the inflow interfaces is considered to be static. The pressure distribution at any outflow interface node is set equal to that of the adjacent node in the flow field. The surrounding waters entering a water body is characterized by a uniform channel flow. The pressure variation at any cross-section of a uniform channel flow may be proved to be hydrostatic by applying the Bernoulli's equation. This equation is applied to two streamlines, one at the top of the channel and the other at an arbitrary depth. Since, in steady, frictionless, one-dimensional, uniform channel flow the constant in the Bernoulli equation is the same for all streamlines, it can be easily shown that the pressure distribution across the channel, as well as the interface between the channel and the impoundment is hydrostatic.

For the surface boundary, the wind effect produces shear at the water surface which is equal to the shear stress in the fluid near the surface as indicated in eqs. (33) and (34) based on the assumption that the wind velocity components are steady and moderate with zero vertical components and the skin coefficients may be taken from experimental measurements [18, 13]. For the lateral solid-fluid and bottom boundaries, the velocity components normal to the boundaries is always zero. The tangential velocity components is calculated by the application of no-slip condition. With this condition, both tangential velocity components at the solid boundary are set equal to zero. The no-slip boundary condition is ideal for very fine grid spacing. However, computational economy requires a coarse grid spacing for most dynamic three-dimensional hydrothermal analyses. Since, a coarse grid does not afford sufficient resolution at the boundary, a limited amount of numerical error will be induced in the solution. For the fluid-fluid boundaries, the velocity distribution at the inflow interfaces is set equal to the channel inflow velocity distribution which is considered to be a known function of time. The velocity distribution at any outflow interface node is set equal to that of the adjacent node in the flow field.

For the surface boundary, the rate of heat dispersion through the water (involving both conduction and turbulent thermal diffusion) is equal to the heat transfer from water to air as indicated in eqs. (32) and (35) based on values of the heat exchange coefficient K and equilibrium water temperature E, both estimated in terms of meteorological conditions [19].

For the lateral solid-fluid and bottom boundaries the heat transfer is considered to be negligible leading to zero temperature gradient at the boundary. The temperature distribution at the fluid-fluid boundaries is treated similar to the velocity distribution. The temperature at the inflow interface is set equal to the channel inflow temperature which is considered to be a known function of time. The temperature at any outflow interface node is set equal to that of the adjacent nodes in the flow field.

The water level at the fluid-fluid boundaries is treated similar to the temperature distribution. The water level at the inflow interface is set equal to the channel inflow water level which is considered to be known. The water level at outflow interface nodes are set equal to that of the adjacent nodes in the flow field. For the lateral solid-fluid, the water level is calculated from vertical velocity components at surface boundary nodes.

In the development of pressure equation, values of $\partial Q_x^*/\partial x^*$ $\partial Q_y^*/\partial y^*$, and $\partial Q_z^*/\partial z^*$ should be evaluated in the flow field. It was shown earlier that variables Q_x^*, Q_y^*, and Q_z^* are related to the velocity field by eqs. (24), (25), and (26). It should be realized that the only spatial derivatives of Q_x^* needed in the present analysis is $\partial Q_x^*/\partial x^*$. Calculation of $\partial Q_x^*/\partial x^*$ in the fluid cell next to the boundary requires the calculation of Q_x^* at the boundaries normal to the x axis. Similarly, calculation of $\partial Q_y^*/\partial y^*$ and $\partial Q_z^*/\partial z^*$ require the calculation of Q_y^* and Q_z^* at the boundaries normal to the y and z axis respectively. For the surface boundary, only Q_z^* is needed. As stated earlier, since the vertical velocity component in the water level element is small, eq. (26) gives

$$(Q_z^*)_{z^* = z_s^*} = - \frac{\rho^*}{F_0^2} \tag{41}$$

For the lateral solid-fluid boundaries, only the component of Q^* normal to the solid boundary is required. Since the velocity component normal to the solid boundary is zero, eq. (25) will,therefore, give

$$(Q_y^*)_{y^* = 0} = (Q_y^*)_{y^* = y^*_{max}} = \frac{\nu_h}{\nu_0} \frac{1}{R_0} \frac{\partial^2 v^*}{\partial x^{2*}} \tag{42}$$

For the bottom boundary only Q_z^* is needed. Simplification of eq. (26) at the bottom boundary gives

$$(Q_z^*)_{z^* = 0} = - \frac{\rho^*}{F_0^2} + \frac{\nu_v}{\nu_0 R_0} \left(\frac{\partial^2 w^*}{\partial z^{*2}}\right) \tag{43}$$

For the fluid-fluid boundary, the surrounding waters entering the water body is characterized by a uniform channel flow, with a uniform velocity at any cross section and zero axial pressure gradient. As an example, application of the momentum equation along the channel flowing in the x-direction gives

$$(Q_x^*)_{x^*=0} = 0 \qquad (44)$$

NUMERICAL SOLUTION

The numerical scheme, used in this study, is mainly based on the application of spatial and temporal finite difference technique to the governing equation described in the previous section. This scheme is divided into the following steps [17]:

1) Initialization and setting of boundary conditions

2) Calculation of vertical velocity component

3) Calculation of pressure distribution

4) Calculation of the time derivatives for the horizontal velocity components and temperature

5) Calculation of the time derivative for the water level, horizontal velocity components and temperature in the water level elements

6) Time integration and updating of the horizontal velocity components and temperature

7) Time integration and updating of the water level, velocity components, and temperature in the water level elements

8) Calculation of density distribution

After the completion of the last step, the problem time is incremented, the computational procedure is repeated starting at the second step, and the integration cycle is continued until the final problem time is reached.

The initial conditions of the problem consist of the initial values of temperature, velocity components, and pressure at time $t = 0$. These quantities are most easily obtained by the application of the present dynamic analysis. To demonstrate this application, let us consider that it is desired to determine the dynamic response of a water body when it is subjected to a prescribed thermal discharge. The solution to the problem can be obtained in two steps. In the first step, the dynamic response is obtained by setting the thermal discharge temperature equal to the river inflow temperature. Maintaining the atmospheric and the inflow conditions unchanged, the water body will reach equilibrium conditions and the pressure, velocity and temperature distribution will be obtained. In the second step, these equilibrium conditions are entered as the initial conditions and the thermal discharge temperature is set equal to the prescribed value. Again, if the atmospheric and inflow

conditions are held unchanged, the water body will reach new equilibrium conditions. An examination of this dynamic response will enable the program user to predict the effects of the thermal discharge on the state of the water body. The results of this study could then be used to determine if the state's allowable temperature standards have been violated. These standards generally vary from state to state. Many states impose a maximum allowable water temperature, a temperature rise, and a rate of temperature rise on the use of water bodies.

From the temporal viewpoint, the boundary conditions stated earlier are of two types -- time-independent and time-dependent. The setting of the time-independent boundary conditions are undertaken prior to the beginning of the dynamic solution. The time-dependent boundary conditions are satisfied during the execution of the integration cycle. For example, the time-dependent boundary conditions on vertical velocity and pressure are satisfied during the execution of steps 2 and 3 stated above, respectively.

Numerical Stability and Convergence

The numerical procedure, presented in the previous section, involves spatial integration for the calculation of the vertical velocity components and pressure, as well as time integrations for the calculation of the horizontal velocity components and temperature. These spatial and time integration procedures are plagued by numerical stability problems caused by round-off errors in the numerical solution and convergence problems caused by the truncation error due to the finite magnitude of the space and time increments. A summary of the results for the selection of space and time increments are presented hereunder [17]:

$$(\Delta x_i + \Delta x_{i-1}) \leqslant \frac{4D_h}{|u|} \tag{45}$$

$$(\Delta y_j + \Delta y_{j-1}) \leqslant \frac{4D_h}{|v|} \tag{46}$$

$$(\Delta z_k + \Delta z_{k-1}) \leqslant \frac{4D_v}{|w|} \tag{47}$$

$$\Delta t \leqslant 1/(8D_h/(\Delta x_i + \Delta x_{i-1})^2 + 8D_h/(\Delta y_j + \Delta y_{j-1})^2 + 8D_v/(\Delta z_k + \Delta z_{k-1})^2) \tag{48}$$

$$\Delta t \leqslant 1/(2|u|/(\Delta x_i + \Delta x_{i-1}) + 2|v|/(\Delta y_j + \Delta y_{j-1})) \tag{49}$$

$|u|$, $|v|$, and $|w|$ are the estimated maximum absolute values of the velocity components which could occur during the transient. It is true that

these values are not known a priori, but an estimate of the maximum values can generally be made.

PRESENTATION OF RESULTS

The mathematical formulation and the computer program, developed in this study, is verified by applying the dynamic analysis to a number of cases where the final steady-state solution is either known experimentally or the flow pattern has been determined by other investigators. These verification studies are considered in the next section.

Verification Studies

The following problems were selected for verification purposes:

1) Experimental studies on the laminar flow development in a square duct [20]

2) Natural circulation in a pond partially heated from the bottom or the side

The first study consists of a duct with a square cross section with a spatially and temporally uniform input velocity at the duct entrance. Since the geometric dimensions of the laboratory model used in the experimental studies were small and our interest here is in water bodies of appreciable size, the similarity between the present and the experimental study is based on two dimensionless parameters: 1) the quotient of aspect ratio x/D to Reynolds number; and 2) the ratio of the fluid velocity to the average inlet velocity. The geometric and hydraulic input data for this case is given in Table I and Fig. 2a. The computational grid used in this dynamic analysis consists of 13 x 5 x 5 mesh points with non-uniform spacing in the longitudinal direction and uniform spacing in the square cross section as shown in Table II. The initial values of the velocity components in the flow field were selected uniform in the longitudinal direction equal to the inlet velocity with zero transversal and vertical velocities. The dynamic solution was continued until the flow pattern in the duct reached steady state. Typical time histories for a number of upstream and downstream points along the duct axial central plane are obtained and used to plot the final steady state centerline and vertical velocity profiles in the square duct. These velocity profiles, in non-dimensional form, are compared in Figs. 2b and 2c with the experimental results of Goldstein and Kreid [20] who measured the laminar flow development in a square duct using laser-doppler flowmeter. This comparison shows that the results of this study are in good agreement with the experimental data. This confirms that the present formulation can predict the three dimensional flow behavior of water bodies.

The second study consists of natural circulation in a pond heated from the bottom or the side with uniform initial temperature, zero initial velo-

cities and zero inlet and outlet mass flux. The geometric and hydraulic input data for this case is given in Table III. The computational grid used in the dynamic analysis consists of 10 x 6 x 6 mesh points with uniform spacing in the longitudinal and transversal directions and non-uniform spacing in the vertical direction. Two cases were examined. In these cases, a step temperature is applied to a portion of side wall or the bottom surface of the pond. The dynamic response of the pond is obtained for each case and the natural circulation flows developed are compared with expected flow patterns. Typical natural circulation flow patterns for partially heated side wall and bottom surface are shown in Figs. 3, 4, 5, and 6 at times t = 40 and t = 25 seconds respectively into the transient. An examination of these flow patterns demonstrates that for the case of partially heated side wall one natural circulation vortex in transversal direction and two symmetric natural circulation vortices in the longitudinal direction are developed which loose their strength as the distance from the heated wall increases (see Figs. 3,4). For the case of partially heated bottom surface, two symmetric natural vortices in vertical-longitudinal and vertical-diagonal planes are developed which loose their strength with increasing distance from the heated surface (see Figs. 5,6). In both cases, described above, the natural circulation vortices formed and the resultant mixing are caused by density differences in the water body. These results establish that the present formulation can predict the three dimensional flow and thermal aspects of water bodies.

Circulation and Stratification in Water Bodies

The present mathematical formulation is applied to the study of circulation and stratification of large water bodies. The water body is considered to be flowing initially at a uniform velocity and temperature and suddenly exposed to a 90° angle jet with higher velocity but the same temperature. This problem is referred to as three-dimensional non-buoyant jet in a cross current. When the dynamic problem reaches steady state, the water jet temperature is suddenly raised to simulate a thermal discharge. This problem is referred to as three-dimensional buoyant jet in a cross current. To facilitate the understanding of the results, the two problems indicated above (i.e. non buoyant and buoyant jets) are discussed separately but the time histories of the results are shown on the same plots for easy reference.

1) Three Dimensional Non-Buoyant Jet in a Cross Current

The problem of a three-dimensional non-buoyant jet in a cross current, as modeled in Fig. 1, was first analyzed. The geometric and hydraulic input data for the case studied are given in Table IV. The water body is assumed to be flowing initially at a uniform velocity of 0.40 ft/sec when suddenly exposed to a jet velocity of 2.00 ft/sec at a 90 degree angle. The surface wind velocity is considered to be zero. Furthermore, the temperature of the thermal discharge is equal to the water body temperature to simulate a non-buoyant jet. A three-dimensional grid was superimposed on the flow field as detailed in Table V. The boundaries of this grid coincide with the physical river boundaries. The nodal points, where

the hydrothermal variables are defined, are located at point ijk of each grid and are shown in Fig. 7. The time histories of the dynamic variables are shown, for points A,B,C,D,E.F,G,and H marked in Fig. 7, as follows:

1) Velocity components and water level for two nodes A and B in front of the incoming jet at the free surface shown in Figs. 8 and 9

2) Velocity components for two nodes C and D in front of the incoming jet at 12.75 feet below the free surface shown in Figs. 10 and 11

3) Velocity components and water level for two nodes E and F located upstream and downstream respectively at the free surface shown in Figs. 12 and 13

4) Velocity components of two nodes G and H located upstream and downstream respectively at 12.75 feet below the free surface shown in Figs. 14 and 15

Examination of the above plots shows the following features:

Considering the flow at the water surface, the transversal velocities at points A and B, in front of the incoming jet, rise initially with a subsequent rise in the vertical velocity leading to a rise in water level in the neighborhood of the incoming jet which in turn affects the field flow conditions as time progresses. Since the total head associated with the jet and river flow entries are constant, on a short term basis an increase in the water level must be accomplished with a corresponding decrease in the field velocity. The disturbance caused by the incoming jet travel from the discharge point both upstream and downstream of the river. This demonstrates the propagation of the surface gravity waves (surge waves). As time progresses, these disturbances reach the river exit and are reflected back upstream. This demonstrates the reflection of the surface gravity waves from the river exit. However, on a long term basis, a further increase in the water level in the neighborhood of the incoming jet causes additional horizontal velocity components for further downstream points which will gradually affect the downstream flow. These flow patterns are observed both in axial and transversal direction as discussed hereunder:

a) The increase in the water level initially decelerates the axial flow on a short term basis. With a further increase in the water level, the axial flow at various points accelerate to their final steady state values which are larger for the downstream points and smaller for the upstream points from the incoming jet position as expected. These effects can be clearly observed in u/U_0 curves for points E, B and F in Figs. 12, 9 and 13 where the transient start with a small dip in the flow rate followed by a steep rise settling to its final steady state value.

b) Similarly, the transversal flow generated by the incoming jet, increases the water level, which in turn, decelerates the transversal flow. However, since, unlike the axial flow patterns, the boundary condition in the transversal direction (solid wall) does not accomodate flow, the trans-

versal flow reaches its final steady state value without undergoing large swings observed in the axial flow curves. These effects can be clearly observed in v/U_0 curves for points A and B in Figs. 8 and 9 where the transversal flow after the initial rise undergoes a reduction in magnitude followed by a mild rise settling to its final steady state values.

At the end of transients discussed above, the increase in transversal flow caused by the incoming jet is accommodated by an increase in the axial flow. For this reason, the water level reaches a steady state value which in turn results in zero vertical velocity and constant axial and transversal flows, observed in Figs. 8 and 9, as the end of non-buoyant analysis is approached.

Examining the flow at 12.76 feet below the water surface, the axial flow exhibit a pattern similar to that of the water surface except that the results are further accentuated due to the bottom boundary condition. Figs. 11, 14 and 15 show that the flow transients u/U_0 start with a relatively large dip followed by relatively smaller rise as it approaches its final steady state value. The effect of the non-slip bottom boundary condition is to reduce the final steady state value to a quantity below that of the surface and to enlarge the initial dip. Furthermore, the shear initiated by the incoming jet creates transversal flow components v/U_0 at this level as observed in Figs. 10 and 11. The transversal flow reduces from the top to the bottom. At the end of transients discussed above, the increase in transversal flow caused by the incoming jet cannot be fully accommodated by an increase in the axial flow in cells near the solids boundaries. For this reason, a downward velocity component develops which induces a vertical downward velocity in the upper cells, observed in w/U_0 curve in Fig. 10. This downward flow extends in a few cells from the jet entrance and is changed to an upwards flow in cells in the center of the flow field.

2) Three Dimensional Buoyant Jet in a Cross Current

The problem of a three-dimensional buoyant jet in a cross current is next analyzed. The geometric and hydraulic input data for this case is exactly similar to the non-buoyant jet case detailed in Fig. 1 and Table IV. The water body is assumed to be initially under the steady state conditions reached in the non-buoyant case discussed earlier when the thermal discharge temperature is suddenly increased from 75°F to 90°F.

The dynamic buoyant jet problem is analyzed in a manner similar to the non-buoyant jet case. However, in view of the introduction of thermal effects, the water body becomes stratified as discussed hereunder. The time histories of the dynamic variables are shown, for points A,B,C,D,E,F,G, and H marked on Fig. 7, as a continuation of the non-buoyant time history plots in Figs. 8 to 15. Examination of these plots shows the following features:

The effect of the heated thermal discharge entering the flow field can be decomposed into two components: 1) unheated discharge entering the flow field studied in the non-buoyant case problem; and 2) thermal effect of the discharge considered in a heated wall studied earlier under the topic of ponds partially heated from the side. According to the above decomposition,

the velocity time history plots on Figs. 8 to 15 for buoyant case should be the sum of the non-buoyant case and the corresponding heated wall problem.

Examining the flow at the water surface at points A and B, in front of the incoming jet, the transversal velocity for the buoyant case shows a small increase in the steady state as compared with the non-buoyant results due to the natural circulation caused by the heated wall. This additional transversal velocity induces an axial velocity transient similar in nature to the non-buoyant case. However, since the magnitude of the transversal velocity transient is small, the resultant axial velocity transient would also be small. This behavior can be clearly observed in u/U_0 and v/U_0 curves in Figs. 8 and 9 which also show the temperature transients T/T_0 for both points A and B. A similar pattern can also be observed at the surface points E and F in Figs. 12 and 13 as well as the points C, G, and H located at 12.75 feet below the water surface in Figs. 10, 14 and 15.

At the end of the transients, the coldest and the hottest regions are at the river and the thermal discharge entrances respectively. For this reason, the strongest natural circulation patterns would develop mainly between these coldest and hottest regions. A comparison of the surface velocity vectors at points A and E and the velocity vectors at 12.75 feet depth for buoyant and non-buoyant cases confirm the existance of this natural circulation pattern. The surface velocity field at the end of the transient is shown in Fig. 16. The slowing down of the entrance flow near the thermal discharge entrance and the turning of the thermal discharge and incoming flows as a result of their interaction can be clearly seen in this figure.

The thermal plume effect is shown in Figs. 17 to 22. Isotherms are plotted for the water surface as well as the vertical planes in the longitudinal and transversal direction at times 60 and 500 seconds after the initiation of the heated discharge. An examination of these plots indicates the following features:

1) The stratification pattern is three dimensional in nature and shows the expansion of the thermal plume in all directions. In view of the prevailing advective currents this expansion is much more intense toward the downstream as compared to the other directions (vertical and upstream) as expected.

2) The three distinctive regions which constitute the characteristic behavior of a stratified water body (epilimnion, thermocline and hypolimnion can be clearly observed in Fig. 22.

3) These results provide the water temperature rise and the rate of temperature rise needed for the assessment of the extent of thermal pollution in the water body.

As a further verification on the validity of the results a mass and energy balance was performed on the water body as shown in Table VI. This table shows that conservation equations are satisfied with a good accuracy. The

small magnitude of the surface heat transfer verifies the often used assumption that, at high values of equilibrium temperature used herein, the contribution of heat exchange to the atmosphere is insignificant and may be neglected in simplified analyses for the purpose of near field studies.

NOMENCLATURE

c_p	Specific heat of water
c_{fx}	Skin coefficient along x-axis
c_{fy}	Skin coefficient along y-axis
d_o	Half width of thermal discharge
D_h	Horizontal eddy diffusivity of heat
D_v	Vertical eddy diffusivity of heat
E	Water equilibrium temperature
F_0	Froud number
g	Gravitional acceleration
H	Water level height in the water level element
K	Heat exchange coefficient for water-air interface
p	Pressure
R_0	Reynolds number
S_0	Stanton number
T_0	Thermal discharge temperature
T	Local water temperature
t	Time
U_0	Thermal discharge velocity
u	Horizontal velocity components in x-direction
v	Horizontal velocity components in y-direction
w	Vertical velocity components in z-direction
W_x	Wind velocity components in x-direction
W_y	Wind velocity components in y-direction
x,y,z	Cartesian coordinate system
Δx_i	Dimension of element i in x-direction
Δy_j	Dimension of element j in y-direction
Δz_k	Dimension of element k in z-direction

Greek Symbols

ρ	Local density of water
ρ_0	Thermal discharge density
ρ_a	Air density
ν_h	Horizontal eddy viscosity
ν_v	Vertical eddy viscosity
ν_0	Thermal discharge kinematic viscosity
∇^2	Laplacian operator $\frac{\partial^2}{\partial x^2} + \frac{\partial^2}{\partial y^2} + \frac{\partial^2}{\partial z^2}$

Superscripts

*	Refers to non-dimensional quantities

Subscripts

0	Refers to thermal discharge
s	Refers to values of variables at the free surface
i,j,k	Indices referring to the location of nodal points along x,y, and z axes respectively

REFERENCES

1. Brady, D.K. and Geyer, J.C., "Development of a General Computer Model for Simulating Thermal Discharge in Three Dimensions", Report No. 7, Cooling Water Studies for Edison's Electric Institute, New York, N.Y., 1972.
2. Liggett, J.A., "Unsteady Circulation in Shallow Homogeneous Lake", Proceedings of the ASCE, Journal of the Hydraulics Division, HY4, July 1969, pp. 1273-1288.
3. Liggett, J.A. and Hadjitheodorou, C., "Circulation in Shallow Homogeneous Lakes", Proceedings of ASCE, Journal of the Hydraulic Division, HY2, March 1969, pp. 609-620.
4. Sengupta, S., "A Three-Dimensional Numerical Model for Closed Basins", ASME Publication No. 76-WA/HT-21, 1976, pp. 1-16.
5. Streeter, V.L., Fluid Mechanics, McGraw-Hill Book Co., Inc., 1958.
6. Hirt, C.W. and Shannon, J.P., "Free-Surface Stress Conditions for Incompressible-Flow Calculations", Journal of Computational Physics, Vol. 2, 1968, pp. 403-411.
7. Waldrop, W.R. and Farmer, R.C., "Three-Dimensional Computation of Buoyant Plumes", Journal of Geophysical Research, Vol. 79, No. 9, March 1974 pp. 1269-1276.
8. Waldrop, W.R. and Farmer, R.C., "Thermal Plumes form Industrial Cooling Water", Proceedings of the 1974 Heat Transfer and Fluid Mechanics Institute, Stanford University Press, 1974.
9. Waldrop, W.R. and Farmer, R.C., "A Computer Simulation of Density Currents in a Flowing Stream", Symposium on Unsteady Flow in Open Channels, BHRA, April 1976.
10. Waldrop, W.R. and Farmer, R.C., "Thermal Effluent-River Interaction", Proceedings Comptes-Rendus, Vol. 3, 1975, Sao Paulo, Brazil, pp. 221-229.
11. Liggett, J.A., "Cell Method for Computing Lake Circulation", Proceedings of ASCE, Journal of the Hydraulics Division, HY3, March 1970, pp. 725-743.
12. Elwin, E.H. and Slotta, L.S., "Streamflow Effects in a Stratified Model Reservoir", ASCE National Water Resources Engineering Meeting, Memphis, Tenn. January 1970.
13. Leendertse, J.J., Alexander, R.C., and Shiao-Kung, L., "Three-Dimensional Model for Estuaries and Coastal Seas", Vol. 1, Principles of Computation, prepared for the Office of Water Resources Research, Department of the Interior R-1417-OWRR, December 1973, Rand, Santa Monica, California.
14. Marchuk, G.I., "About Formulation of Problems on the Dynamics of the

Ocean", International Symposium on Stratified Flows, Novosibirsk, 1972.
15. Harleman, Donald, R.F., "Thermal Stratification Due to Heated Discharges", International Symposium of Stratified Flows, Novosibirsk, 1972.
16. Harlow, F.H. and Welch, J.E., "Numerical Calculation of Time-Dependent Viscous Incompressible Flow of Fluid with Free Surface", Los Alamos Scientific Laboratory, Los Alamos, N.M., 1965.
17. Borhani, M.A., "Thermal Stratification and Circulation of Water Bodies Subjected to Thermal Discharges", Doctoral Dissertation, New Jersey Institute of Technology, 1977.
18. Liu, H. and Presez, H.J., "Wind-Induced Circulation in Shallow Water", Proceedings of ASCE, Journal of the Hydraulics Division, HY7, July 1971, pp. 923-935.
19. Edinger, J.E., Brady, D.K., and Geyer, J.C., "Heat Exchange and Transport in the Environment", Report No. 14, Cooling Water Discharges, Edison Electric Institute, New York, 1974.
20. Goldstein, R.J. and Kried, O.K., "Measurement of Laminar Flow Development in a Square Duct Using a Laser-Doppler Flowmeter", Journal of Applied Mechanics, ASME Vol. 34, 1976, pp. 813-818.

TABLE I - THE GEOMETRIC AND HYDRAULIC INPUT DATA FOR LAMINAR FLOW IN A SQUARE DUCT

Specifications	Dimensions	
	British Unit	SI Unit
Water Body Length	280 ft	85.34 m
Water Body Width	72 ft	21.946 m
Water Body Depth	72 ft	21.946 m
Inlet Water Velocity	1 ft/sec	0.3048 m/sec
Water Temperature	75 ^{o}F	23.89 ^{o}C
Reynolds Number, R_0	20.83	20.83
Hydraulic Diameter of Square Duct, D	72 ft	21.946 m

TABLE II - GRID DIMENSIONS FOR THE LAMINAR FLOW IN A SQUARE DUCT

Element No.	x		y		z	
	ft	m	ft	m	ft	m
1	10	3.048	18	5.486	18	5.486
2	10	3.048	18	5.486	18	5.486
3	10	3.048	18	5.486	18	5.486
4	10	3.048	18	5.486	18	5.486
5	20	6.096	18	5.486	18	5.486
6	30	9.144				
7	30	9.144				
8	30	9.144				
9	30	9.144				
10	30	9.144				
11	30	9.144				
12	30	9.144				
13	30	9.144				

TABLE III - GEOMETRIC AND HYDRAULIC INPUT DATA FOR PARTIALLY HEATED POND

Specifications	Dimensions			
	British Unit		SI Unit	
Water Body Length	540	ft	164.592	m
Water Body Width	250	ft	76.2	m
Water Body Depth	20.5	ft	6.248	m
Water Body Temperature	75	^{o}F	23.89	^{o}C
Water Body Equilibrium Temperature	74	^{o}F	23.33	^{o}C
Temperature of Heated Area	100	^{o}F	37.77	^{o}C
Reference Velocity, U_0	1	ft/sec	0.3048	m/sec
Reference Length, d_0	50	ft	15.24	m
Reference Temperature, T_0	100	^{o}F	37.77	^{o}C
Reference Time, t_0	50	sec	50	sec
Reference Density, ρ_0	61.9963	lbm ft^{-3}	960.590	kg m^{-3}
Reference Pressure, p_0	21.52	lbf in^{-2}	14639.4	kg m^{-2}
Reynolds Number, R_0	0.6061	x 10^7	0.6061 x	10^7
Heat Exchange Coeff., K	100	Btu/ft^2day^{o}F	23.64	W/$m^2{}^{o}C$

TABLE IV - GEOMETRIC AND HYDRAULIC INPUT DATA FOR THREE-DIMENSIONAL, NON-BUOYANT AND BUOYANT JETS IN A CROSS CURRENT

Specifications	Dimensions			
	British Unit		SI Unit	
Water Body Length	600	ft	182.88	m
Water Body Width	360	ft	109.73	m
Water Body Depth	16.5	ft	5.03	m
Jet Width, 2 d_0	100	ft	30.48	m
Jet Depth	5.75	ft	1.75	m
Jet Velocity, U_0	2	ft/sec	.61	m/sec
River Velocity	.4	ft/sec	.12	m/sec
Water Body Temperature	75	^{o}F	23.89	^{o}C
Water Body Equilibrium Temperature	74	^{o}F	23.33	^{o}C
Thermal Discharge Temperature, T_0	90	^{o}F	32.22	^{o}C
Reference Time, t_0	25	sec	25	sec
Reference Density, ρ_0	62.1156	lbm ft^{-3}	962.730	kg m^{-3}
Reference Pressure, p_0	21.56	lbf in^{-2}	14672.0	kg m^{-2}
Reynolds Number, R_0	0.1212	x 10^8	0.1212 x	10^8
Heat Exchange Coeff., K	100	Btu/ft^2day^{o}F	23.64	W/$m^2{}^{o}C$

TABLE V - GRID DIMENSIONS FOR THREE DIMENSIONAL NON-BUOYANT AND BUOYANT JETS IN A CROSS CURRENT

Element No.	x		y		z	
	ft	m	ft	m	ft	m
1	65	19.81	50	15.24	3.5	1.07
2	60	18.29	50	15.24	4.0	1.22
3	55	16.76	55	16.76	5.0	1.52
4	50	15.24	60	18.29	4.0	1.22
5	50	15.24	65	19.81	3.5	1.07
6	55	16.76	70	21.34		
7	60	16.76	70	21.34		
8	65	19.81				
9	70	21.34				
10	70	21.34				

TABLE VI - MASS AND ENERGY BALANCE

Mass or Energy Balance	Incoming Flow	Thermal Discharge	Outgoing Flow	Surface Flow	Percent Error
Mass Balance, in 10^6 lbm/sec	0.12252	0.08464	0.20748	0.0	0.15
Energy Balance, in 10^8 Btu/sec	0.09189	0.07454	0.16204	0.15096 x 10^{-4}	0.18

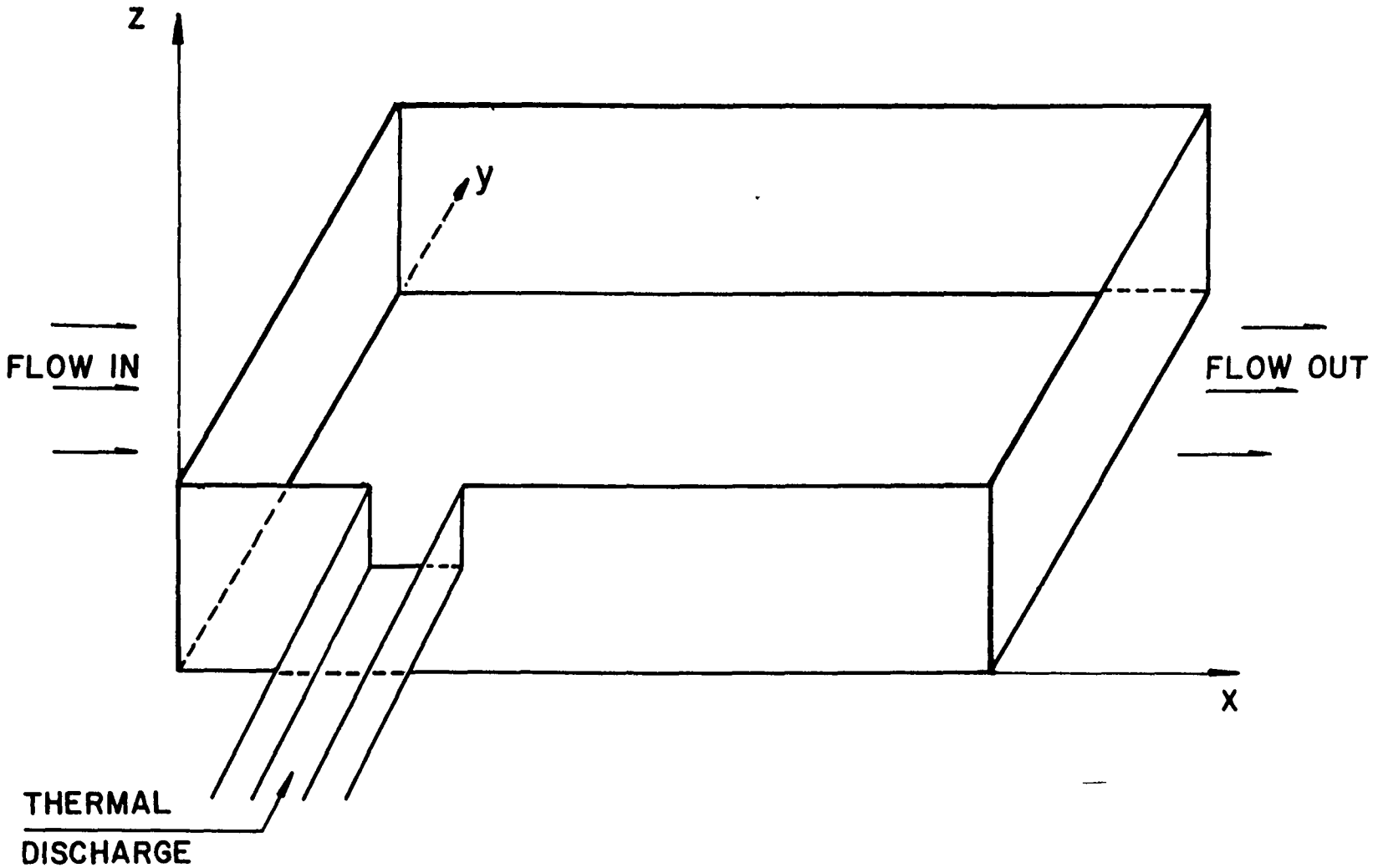

FIG 1. SCHEMATIC DIAGRAM OF THE WATER BODY

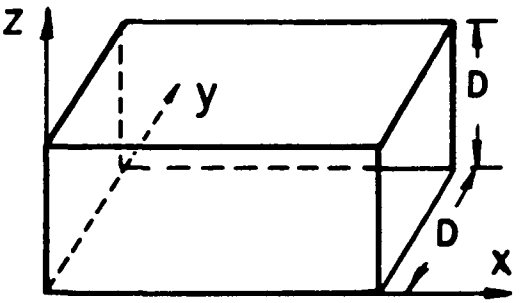

(a) THE SQUARE DUCT CONFIGURATION

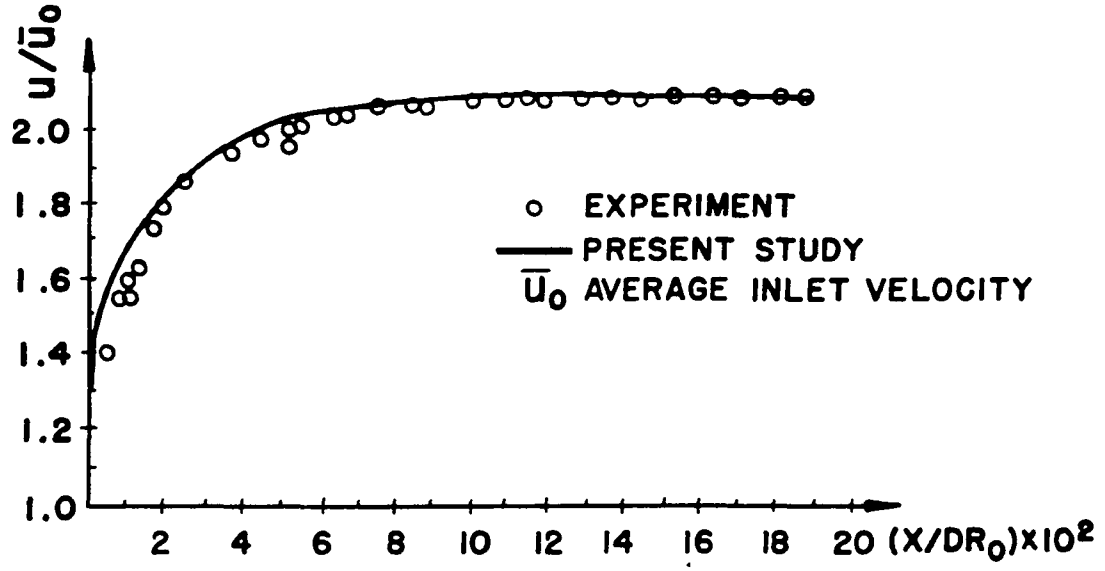

(b) CENTER-LINE VELOCITY DEVELOPMENT

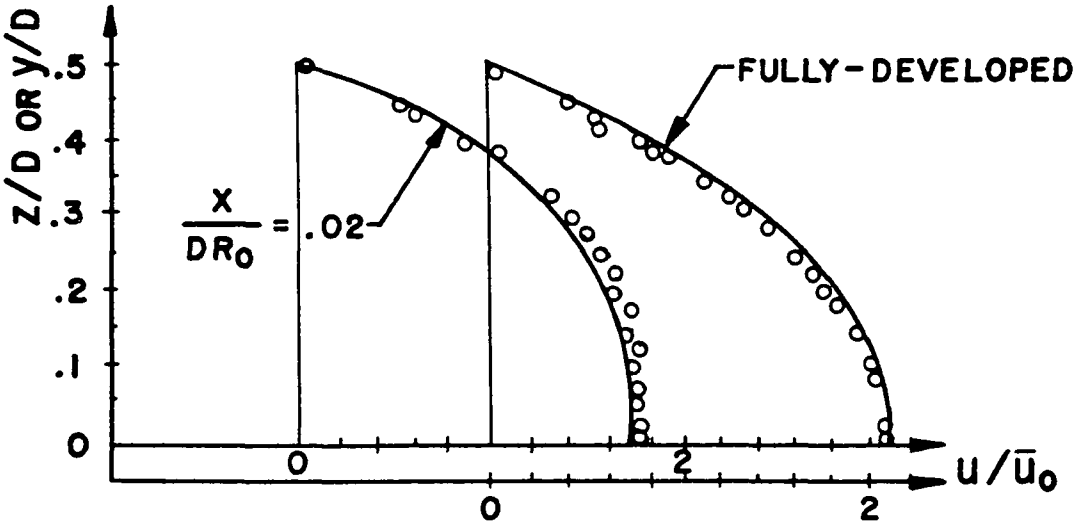

(c) DEVELOPMENT OF VELOCITY PROFILE CENTRAL PLANE

FIG 2. VELOCITY DEVELOPMENT IN A SQUARE DUCT

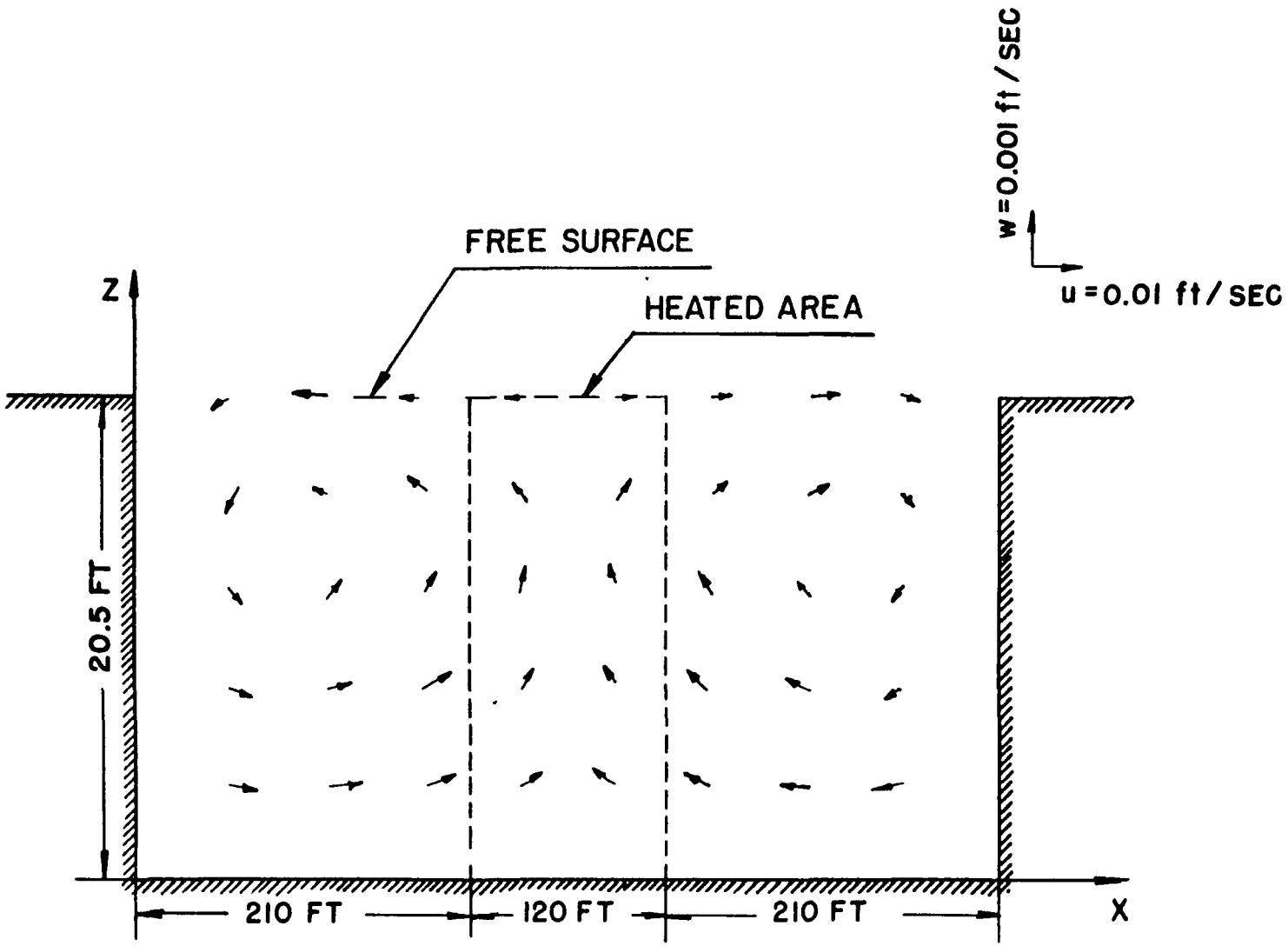

FIG 3. NATURAL CIRCULATION AT y=100 FT. AND t=40 SEC IN A POND PARTIALLY HEATED FROM SIDE.

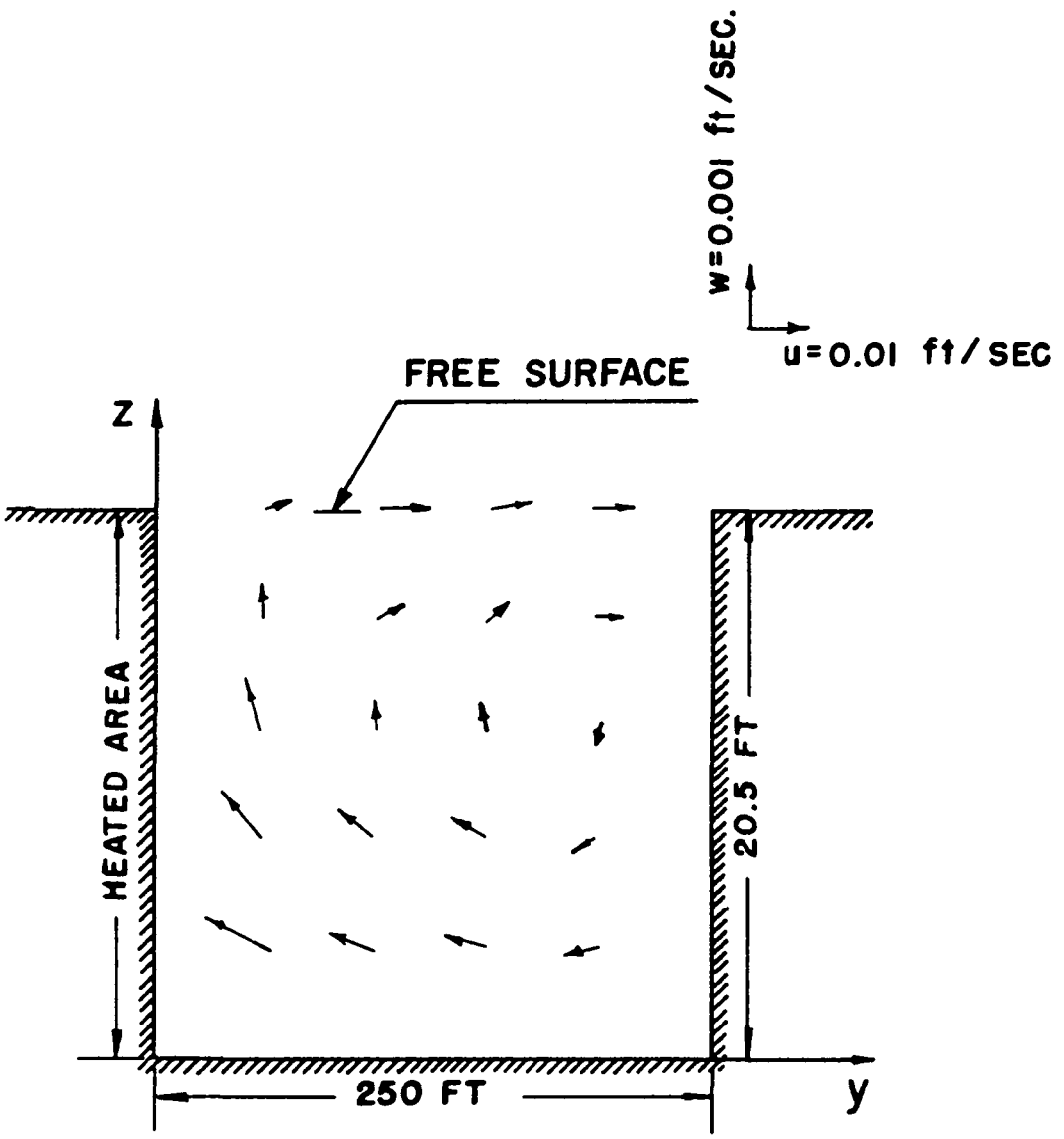

FIG 4. NATURAL CIRCULATION AT X=240 FT. AND t=40 SEC. IN A POND PARTIALLY HEATED FROM SIDE.

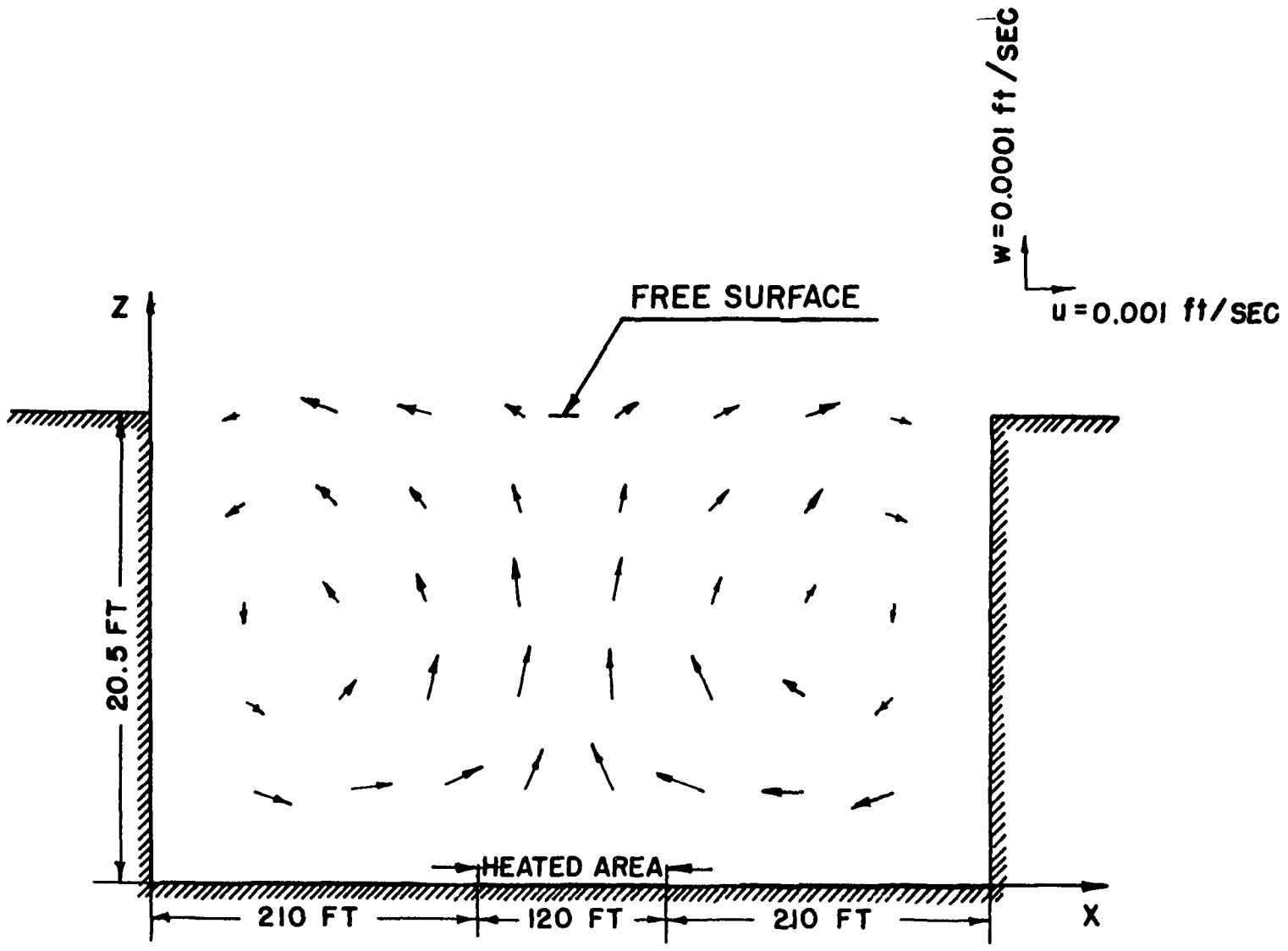

FIG 5. NATURAL CIRCULATION AT y=100 FT. AND t= 25 SEC. IN A POND PARTIALLY HEATED FROM BOTTOM.

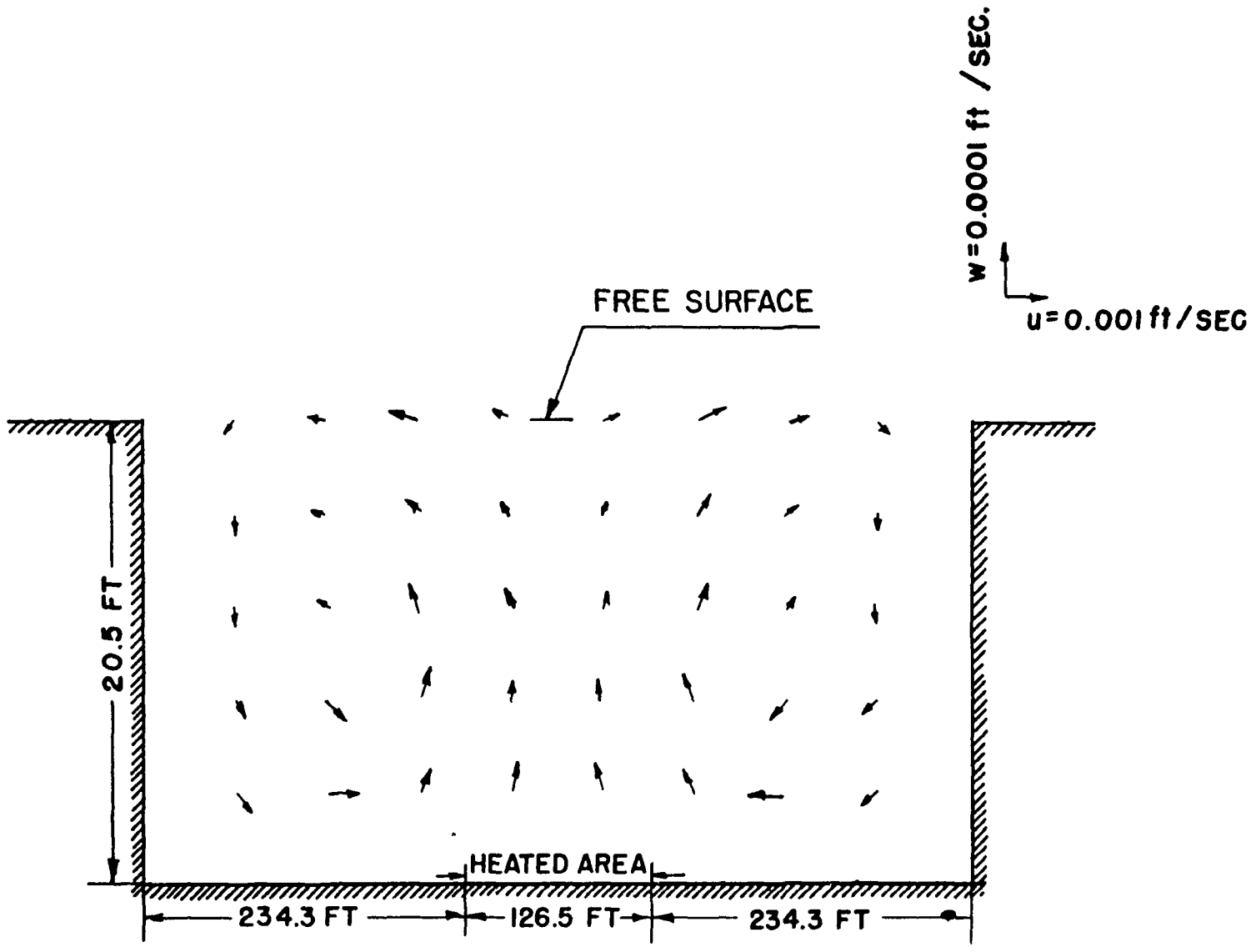

FIG 6. NATURAL CIRCULATION AT $t = 25$ SEC IN VERTICAL DIAGONAL PLANE IN A POND PARTIALLY HEATED FROM BOTTOM

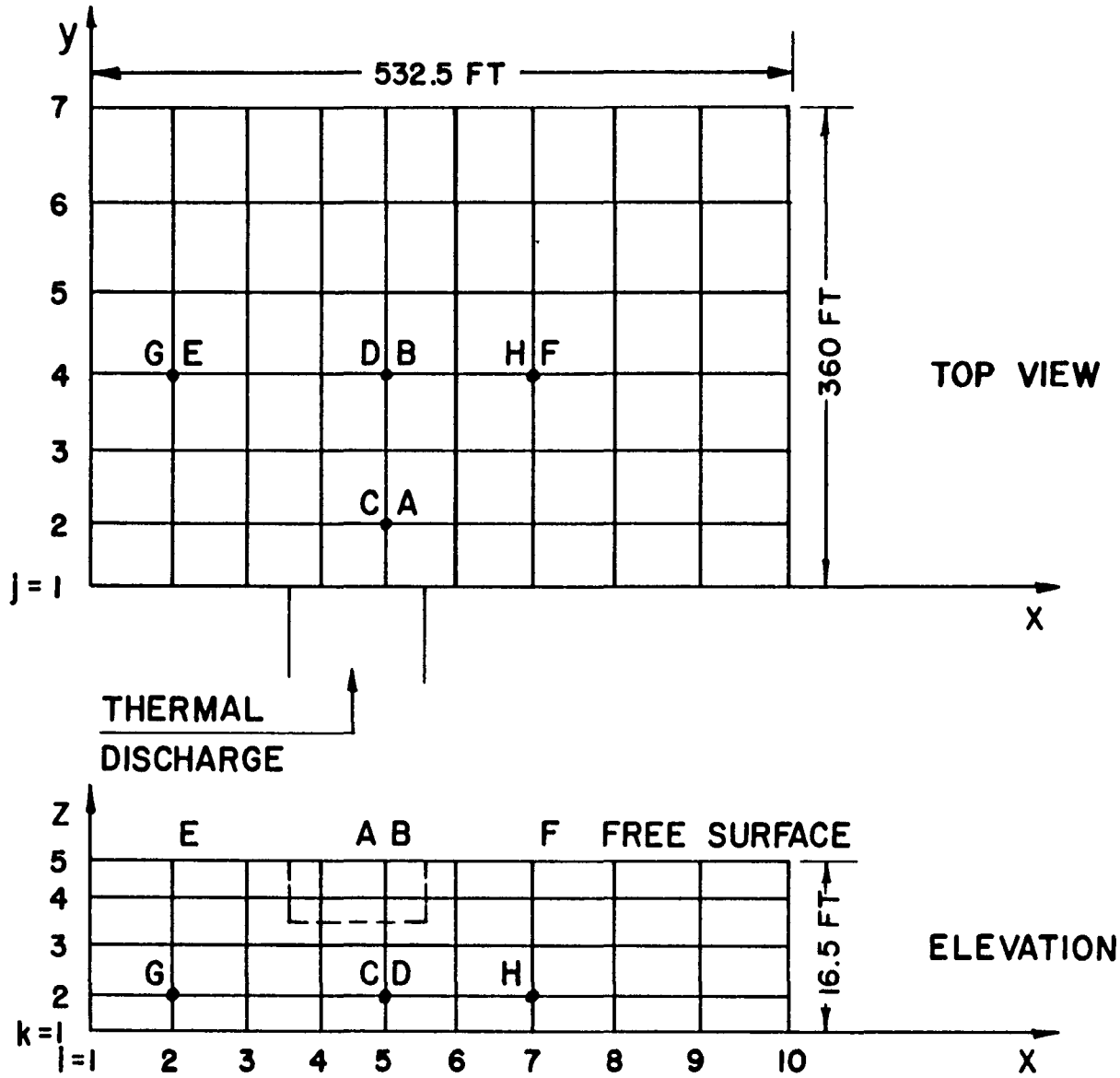

FIG 7. GRID WORK WITH VARIABLE MESH SIZE SUPERIMPOSED ON THE WATER BODY

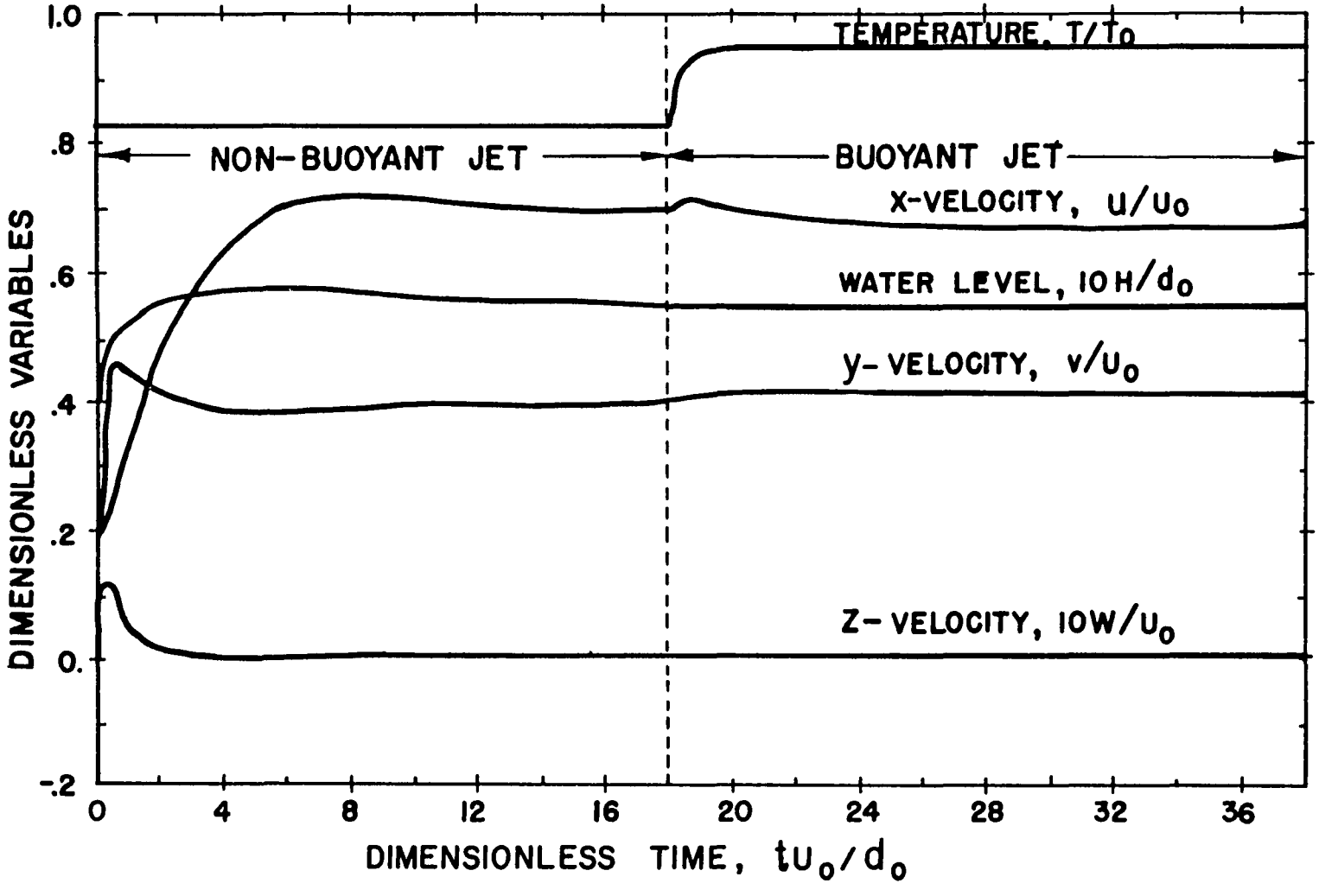

FIG 8. TIME HISTORIES OF VARIABLES AT POINT "A" IN THE WATER BODY SUBJECTED TO NON-BUOYANT AND BUOYANT JETS

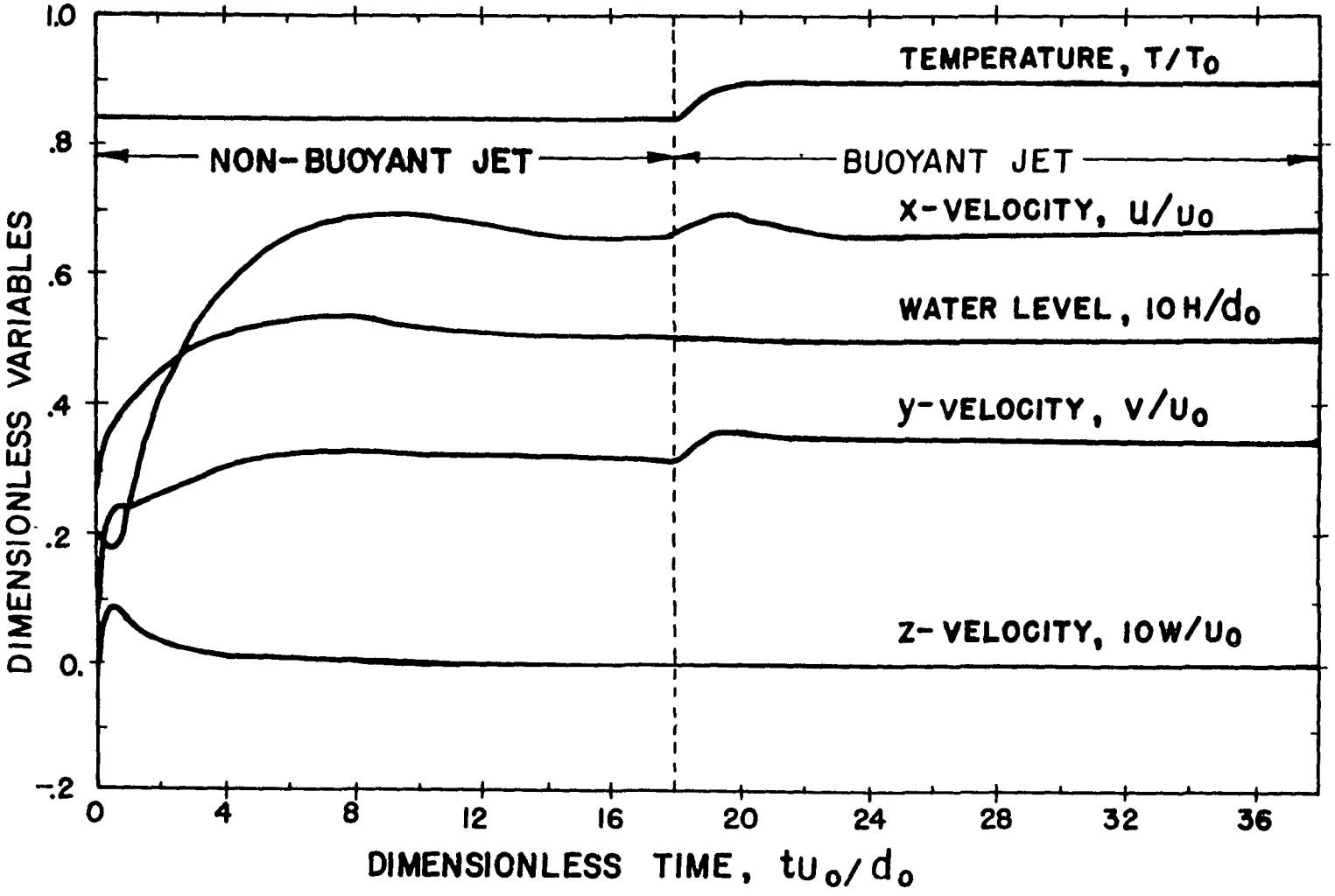

FIG 9. TIME HISTORIES OF VARIABLES AT POINT "B" IN THE WATER BODY SUBJECTED TO NON-BUOYANT AND BUOYANT JETS

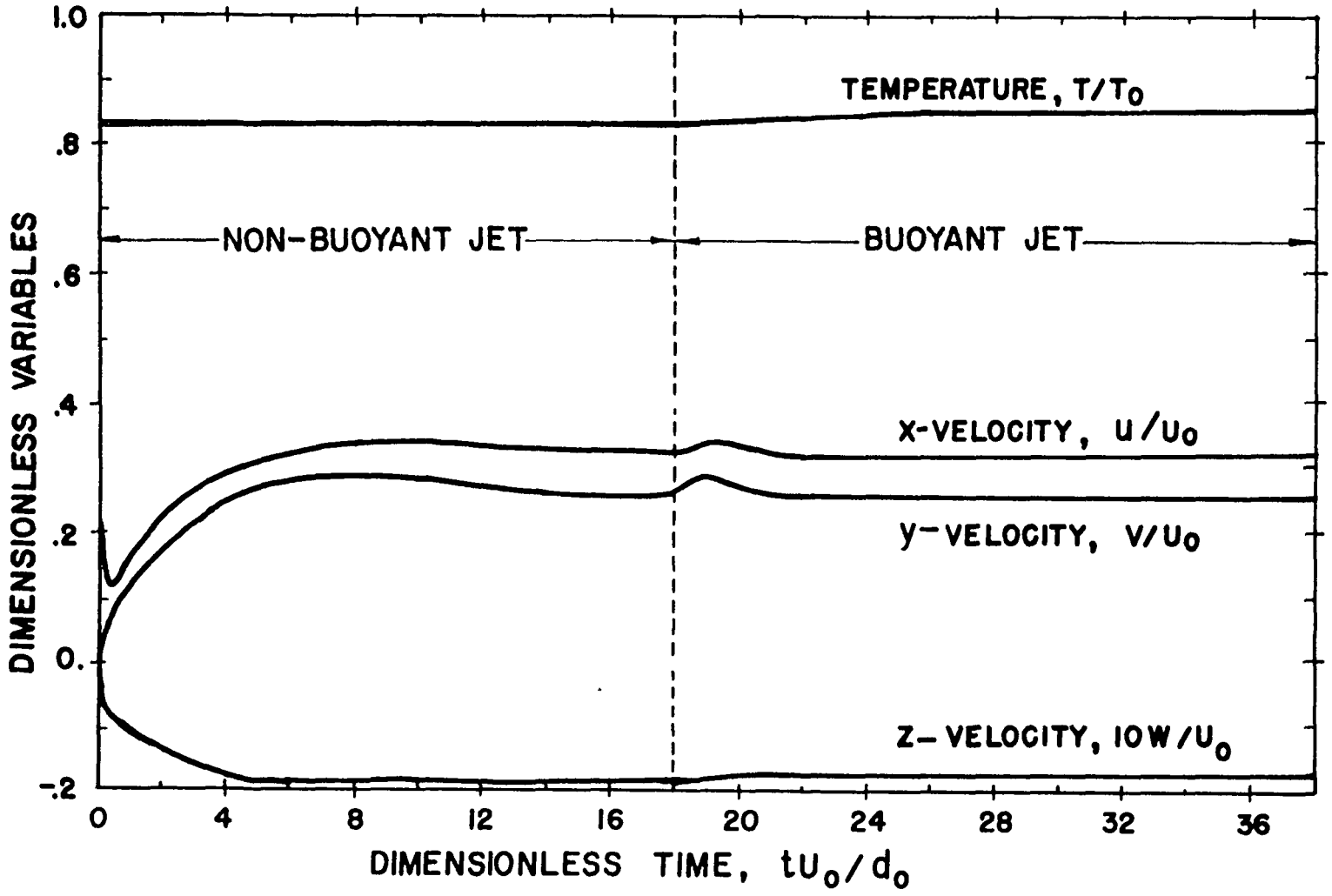

FIG 10. TIME HISTORIES OF VARIABLES AT POINT "C" IN THE WATER BODY SUBJECTED TO NON-BUOYANT AND BUOYANT JETS

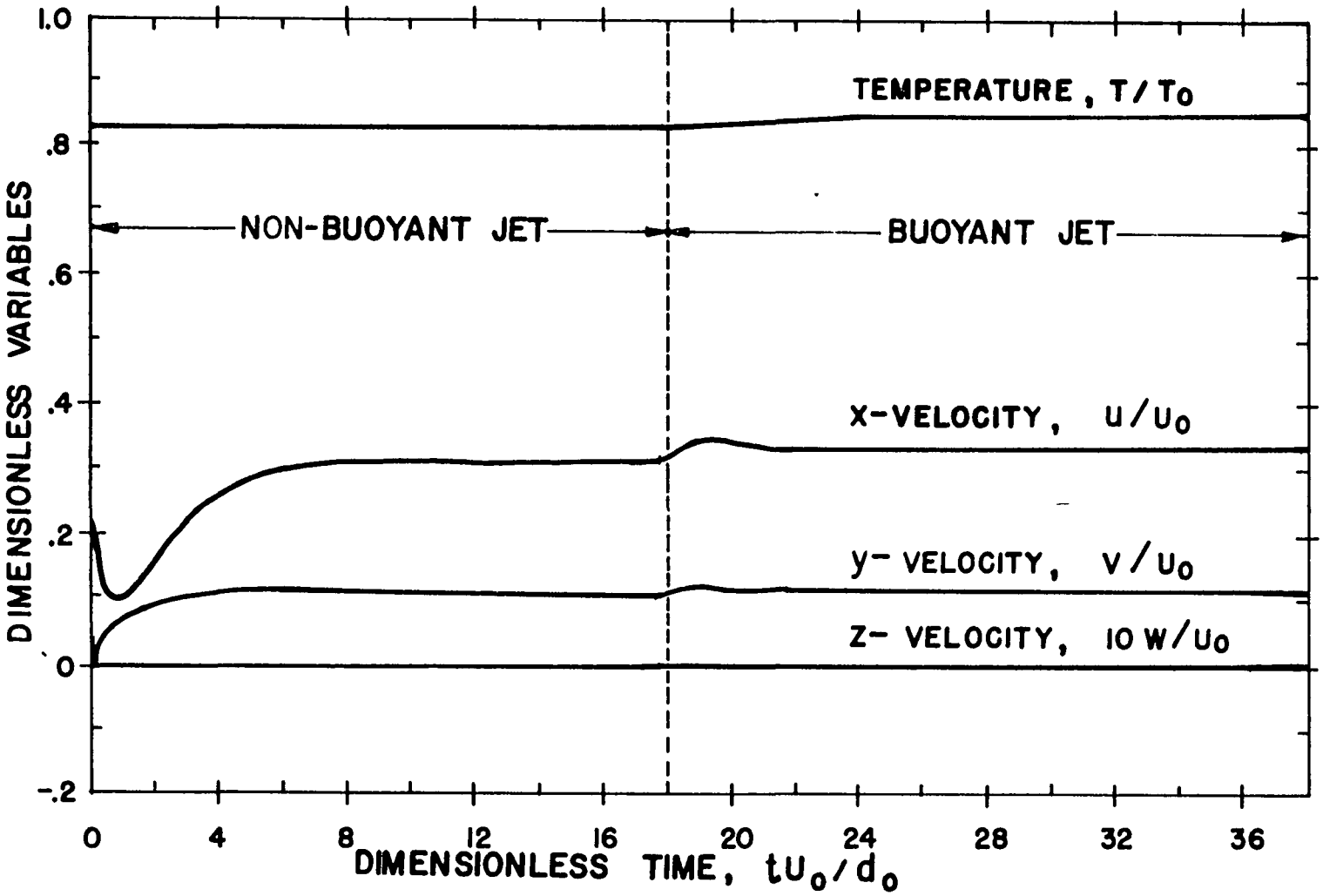

FIG 11. TIME HISTORIES OF VARIABLES AT POINT "D" IN THE WATER BODY SUBJECTED TO NON-BUOYANT AND BUOYANT JETS

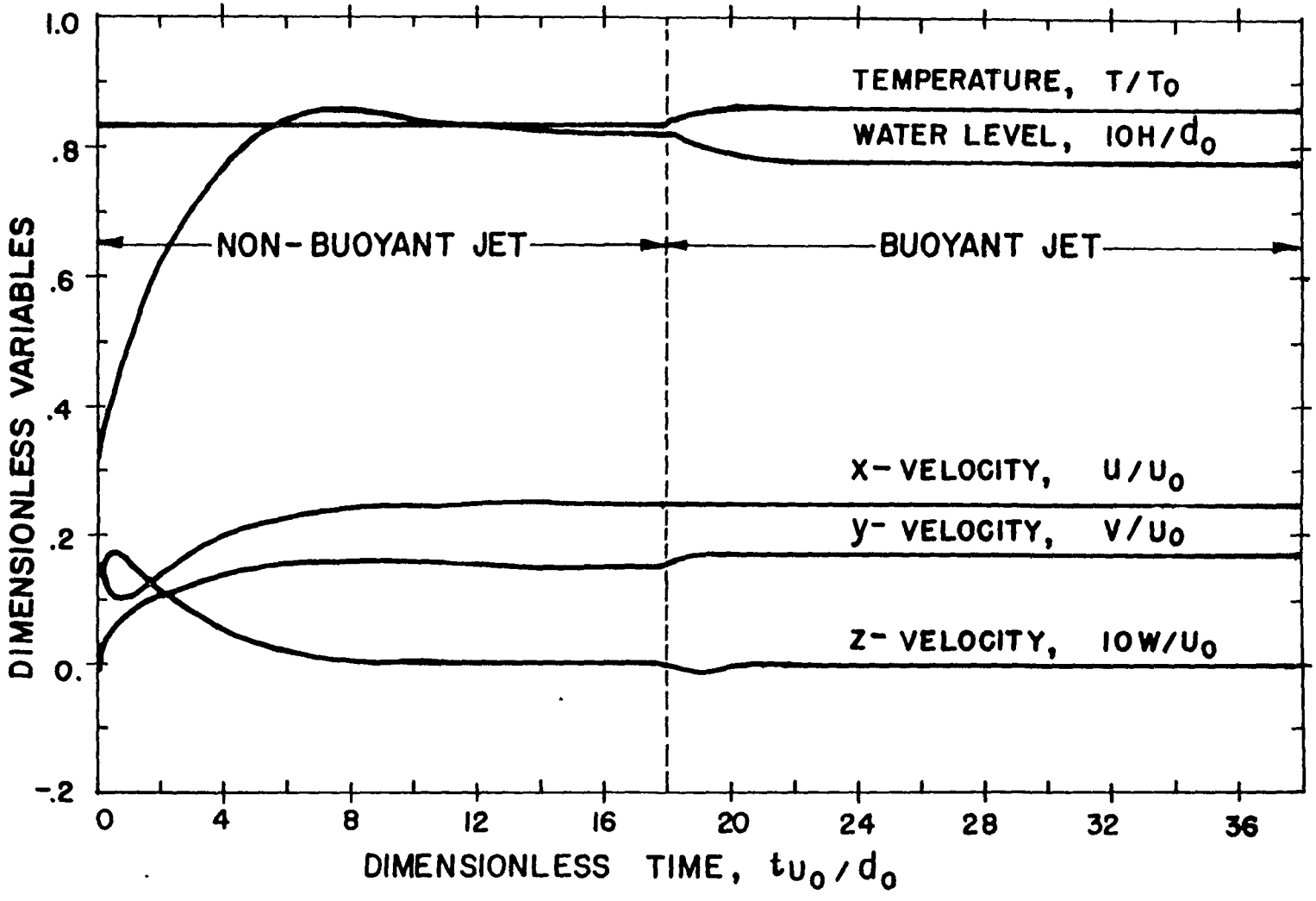

FIG 12. TIME HISTORIES OF VARIABLES AT POINT "E" IN THE WATER BODY SUBJECTED TO NON-BUOYANT AND BUOYANT JETS

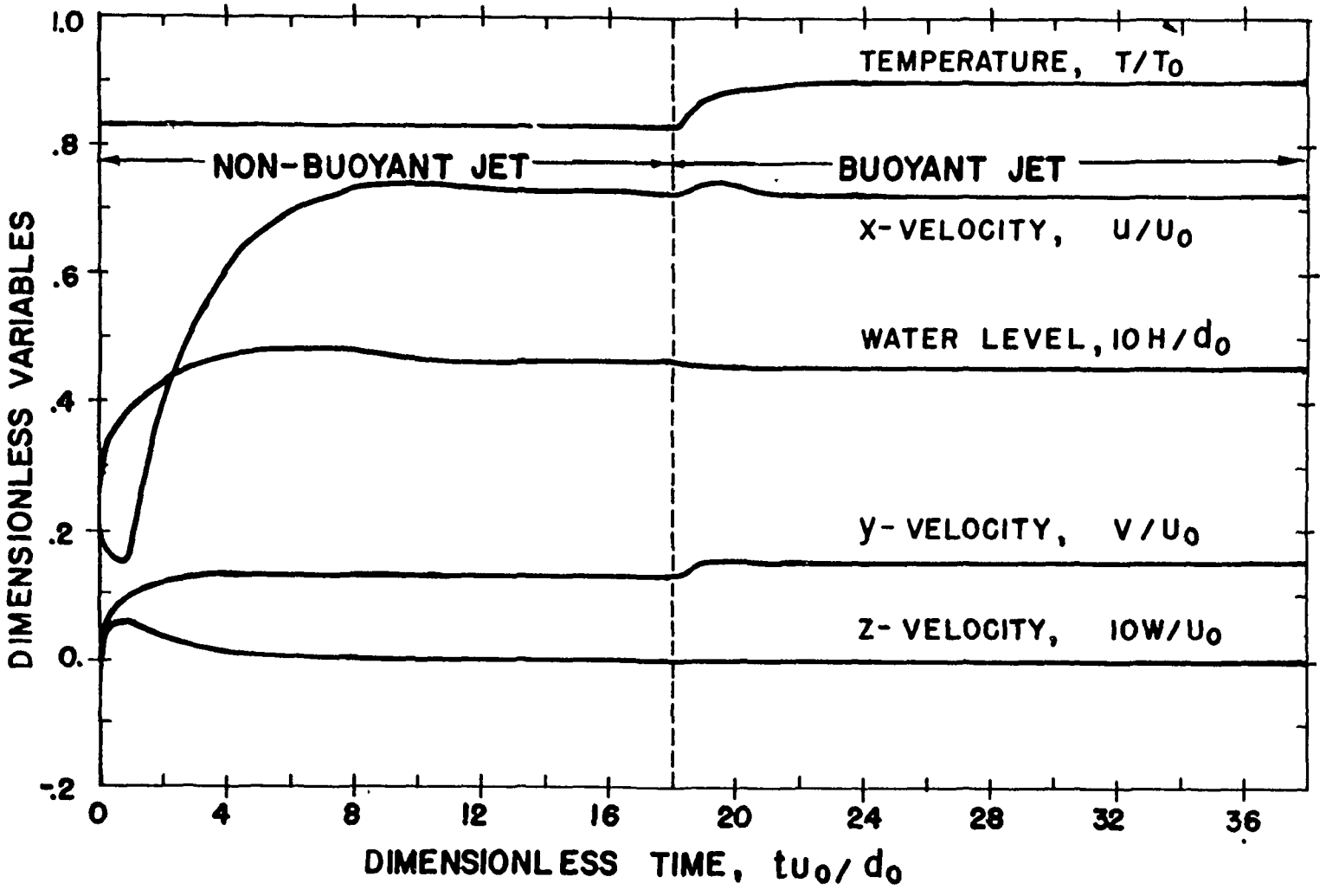

FIG 13. TIME HISTORIES OF VARIABLES AT POINT "F" IN THE WATER BODY SUBJECTED TO NON-BUOYANT AND BUOYANT JETS

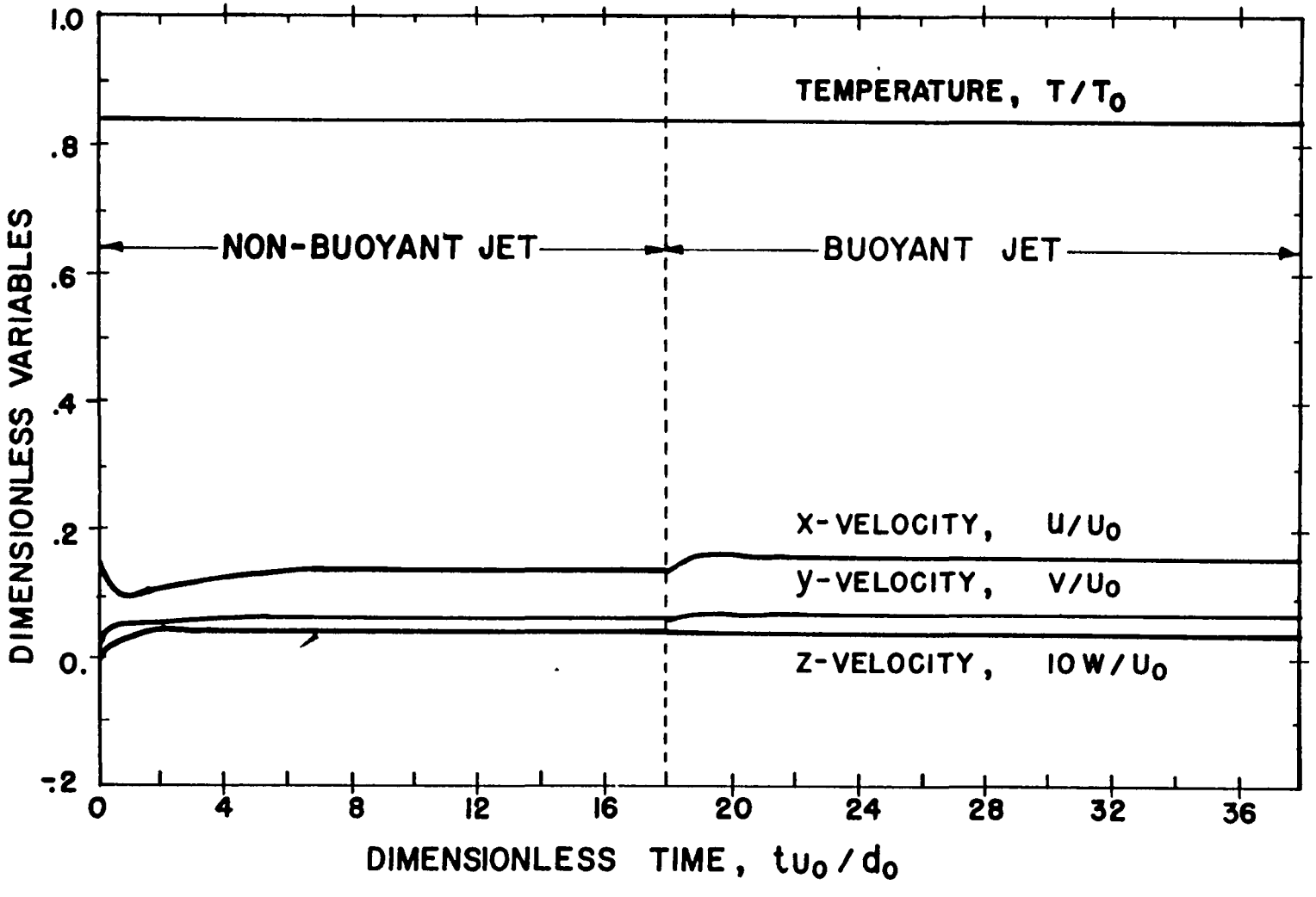

FIG 14. TIME HISTORIES OF VARIABLES AT POINT "G" IN THE WATER BODY SUBJECTED TO NON-BUOYANT AND BUOYANT JETS

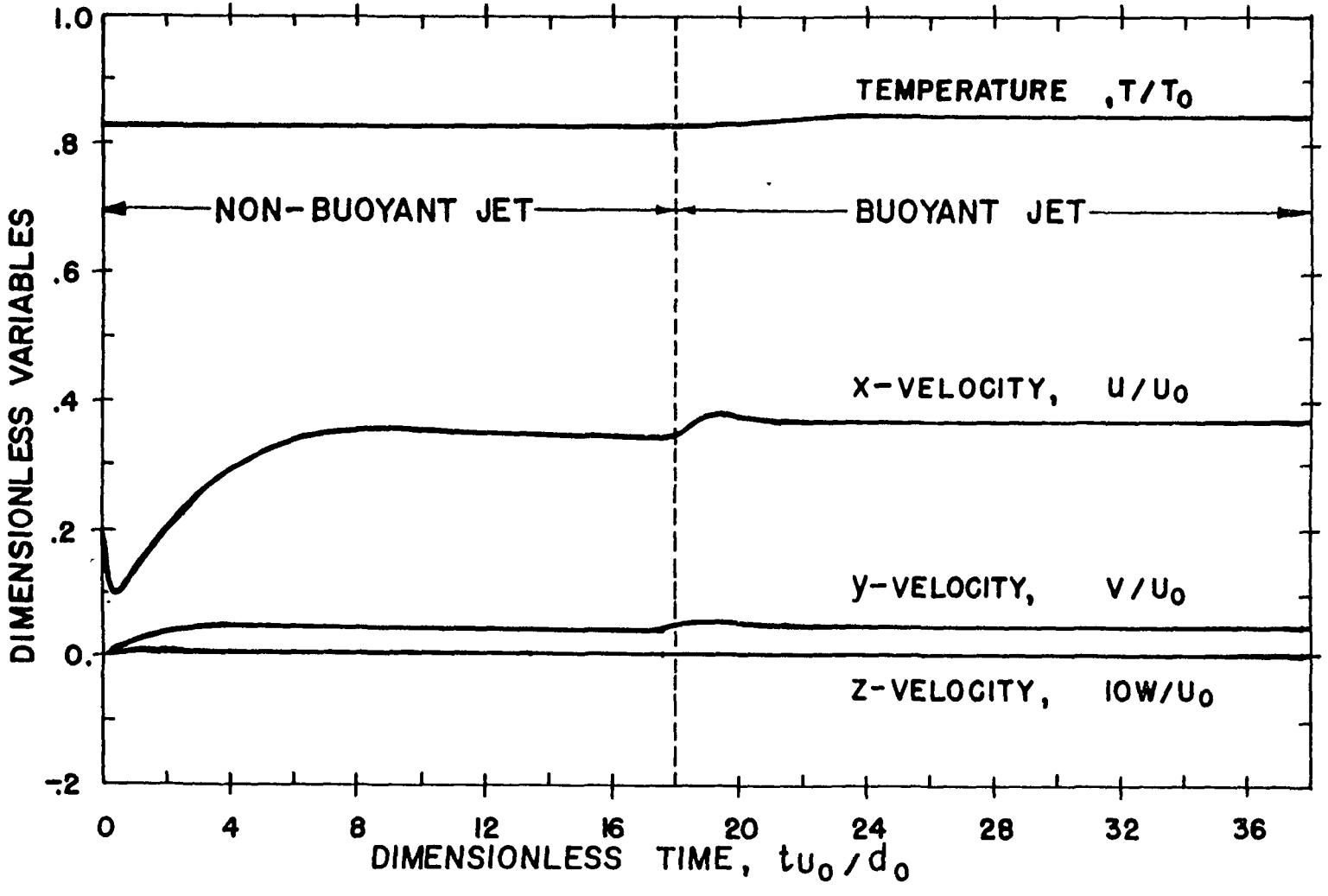

FIG 15. TIME HISTORIES OF VARIABLES AT POINT "H" IN THE WATER BODY SUBJECTED TO NON-BUOYANT AND BUOYANT JETS

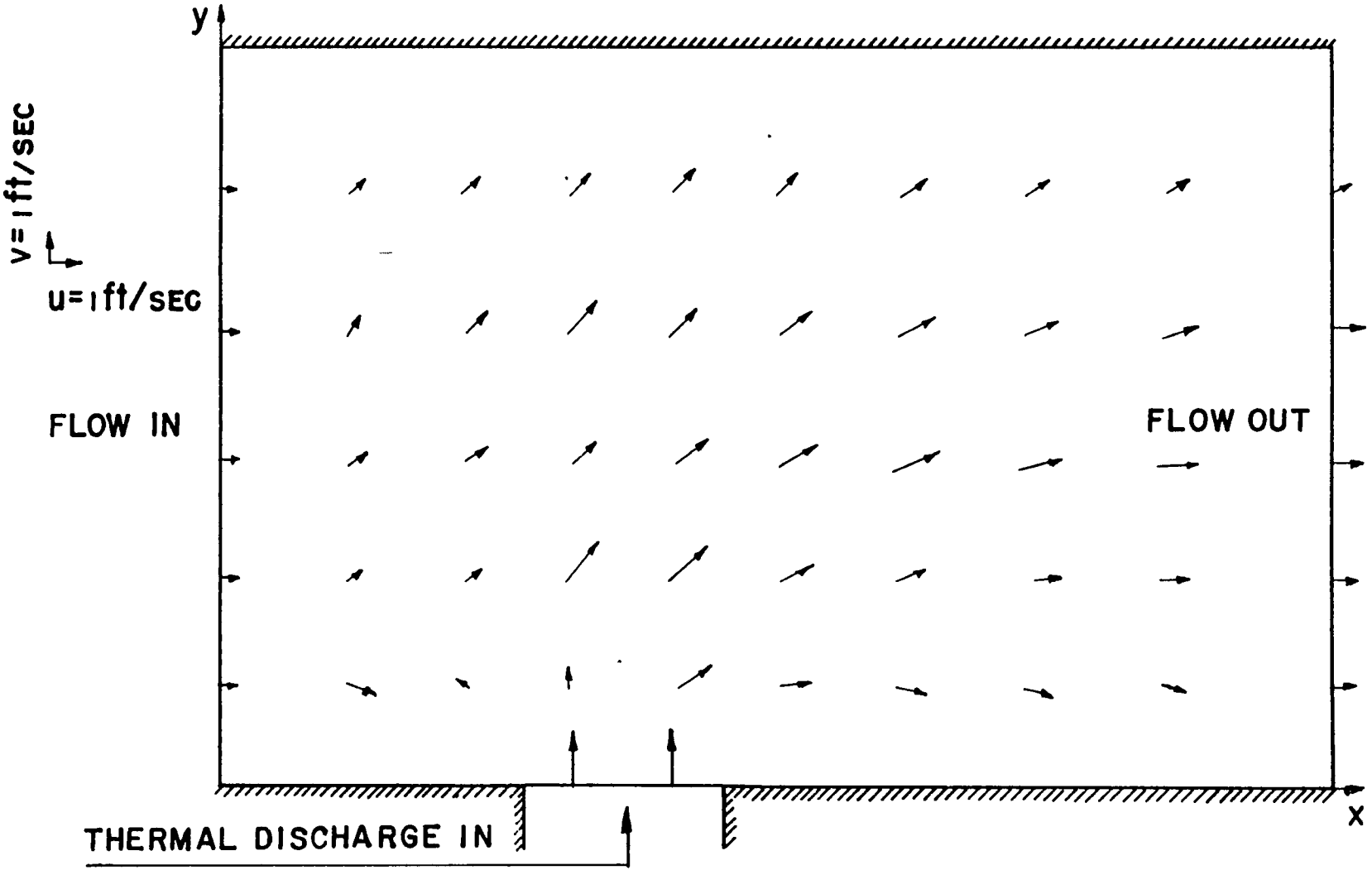

FIG 16. SURFACE VELOCITY FIELD AT $t = 500$ SEC. IN THE WATER SUBJECTED TO A BUOYANT JET

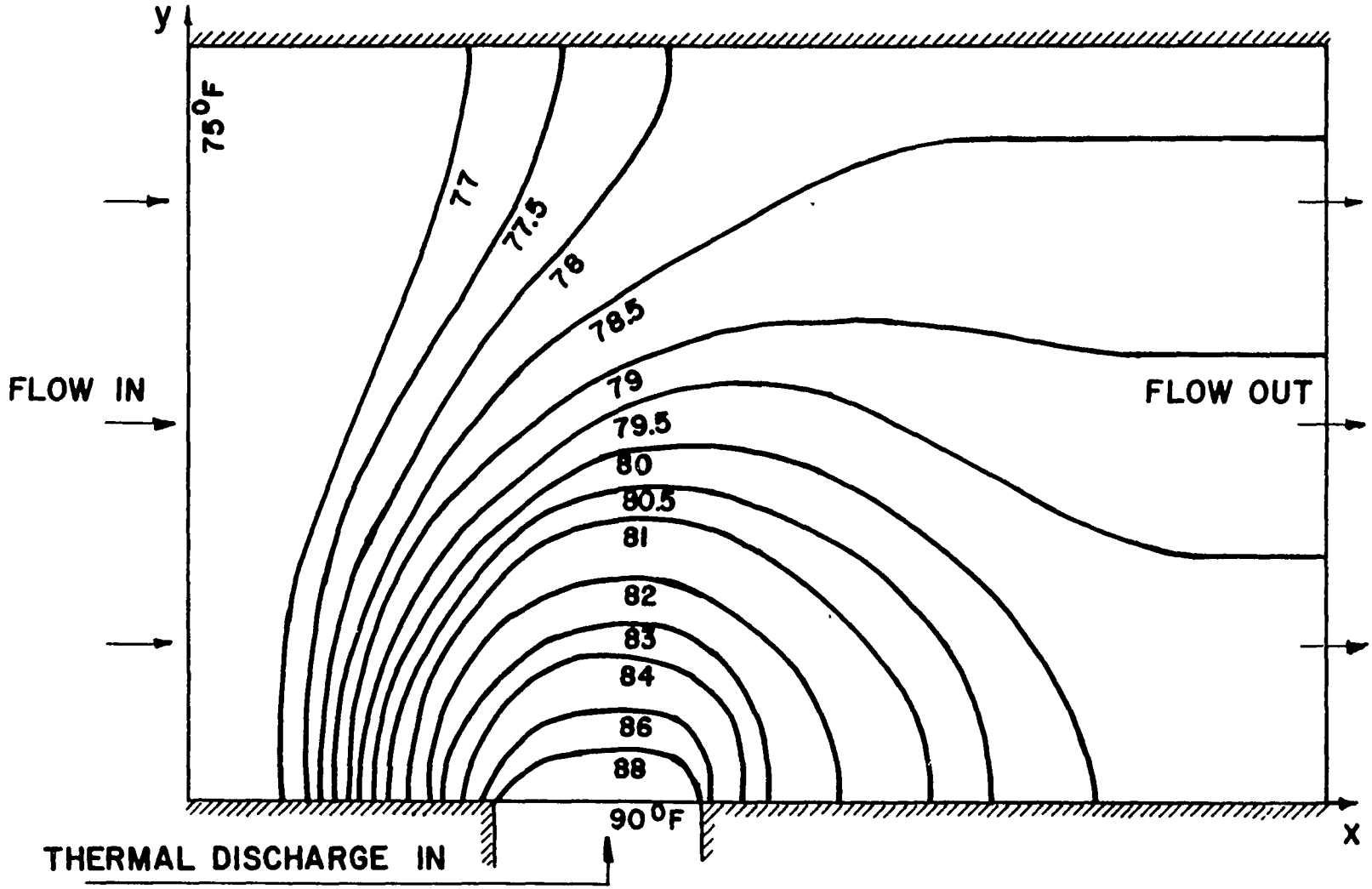

FIG 17. SURFACE ISOTHERMS AT t = 60 SEC. IN THE WATER BODY SUBJECTED TO A BUOYANT JET

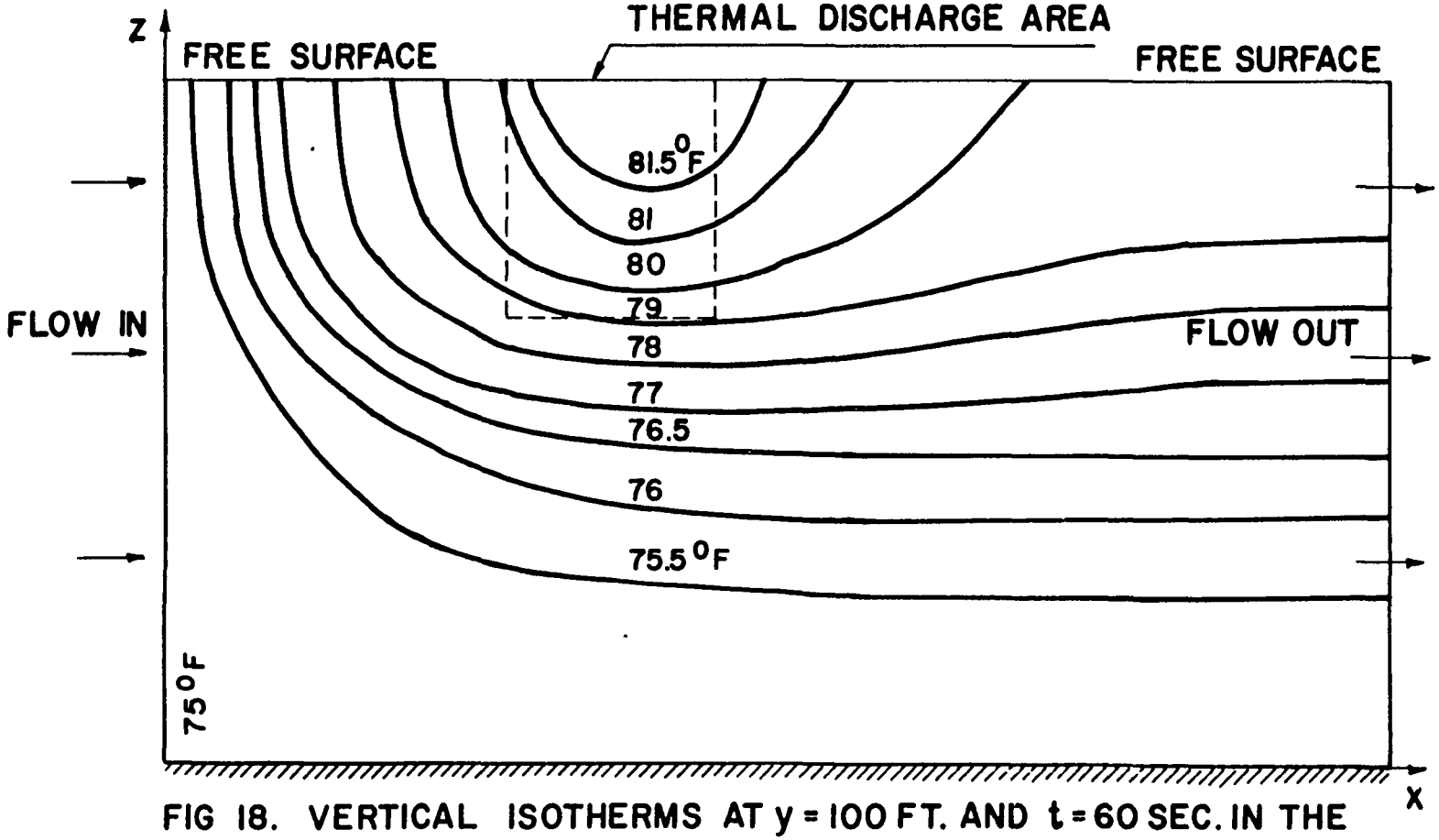

FIG 18. VERTICAL ISOTHERMS AT y = 100 FT. AND t = 60 SEC. IN THE WATER BODY SUBJECTED TO A BUOYANT JET

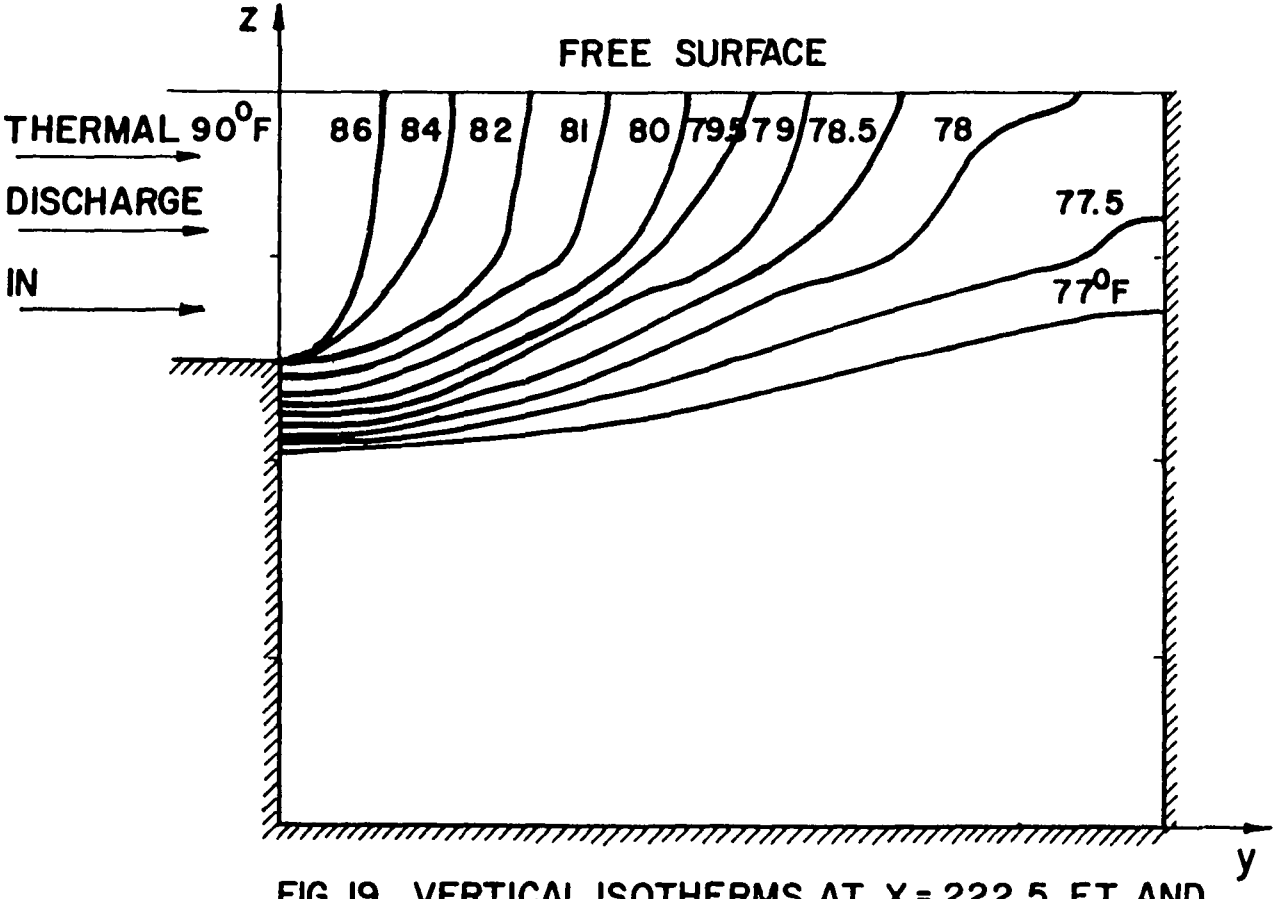

FIG 19. VERTICAL ISOTHERMS AT X = 222.5 FT. AND t = 60 SEC. IN THE WATR BODY SUBJECTED TO A BUOYANT JET

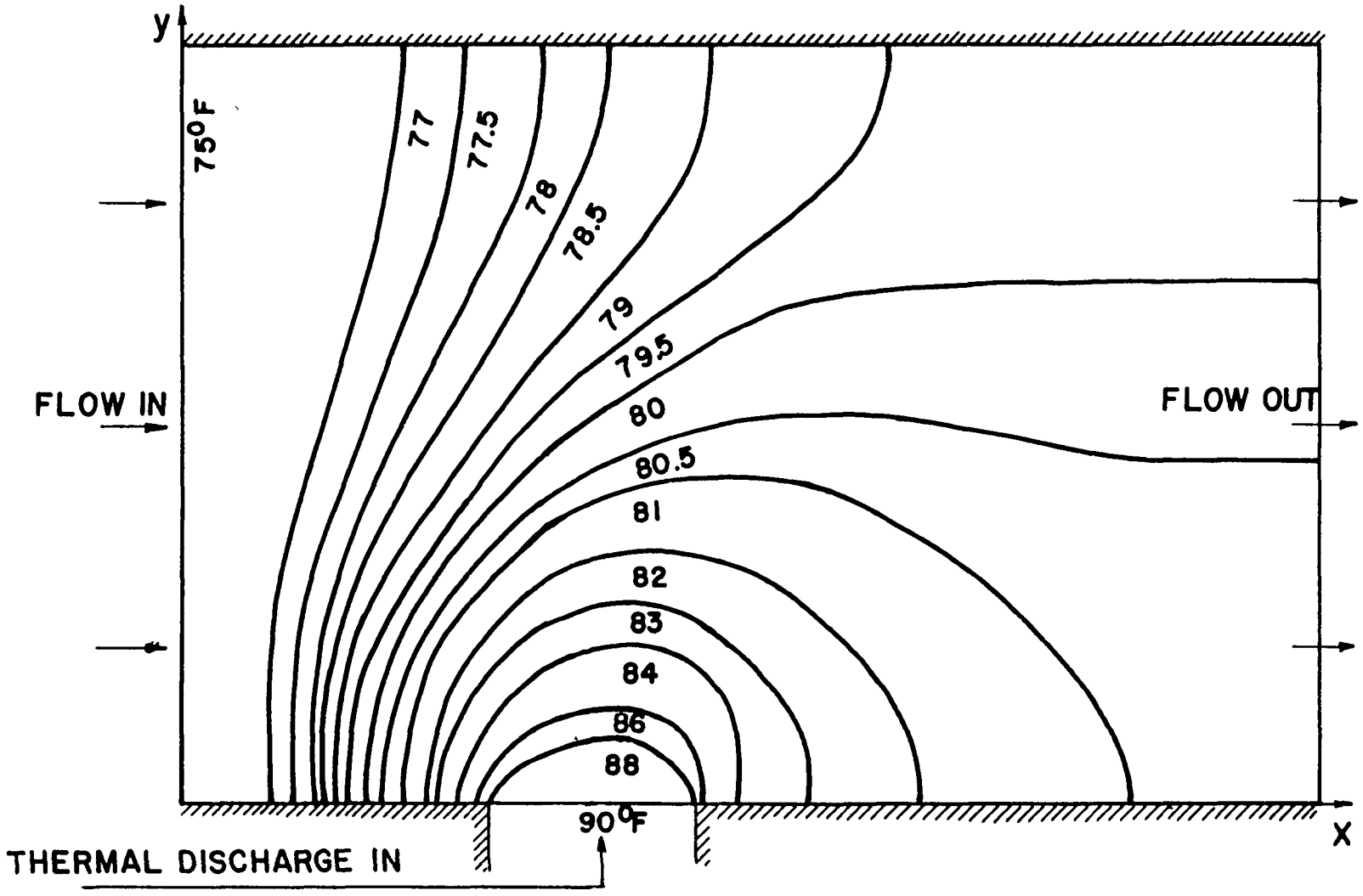

FIG 20. SURFACE ISOTHERMS AT t= 500 SEC. IN THE WATER BODY SUBJECTED TO A BUOYANT JET

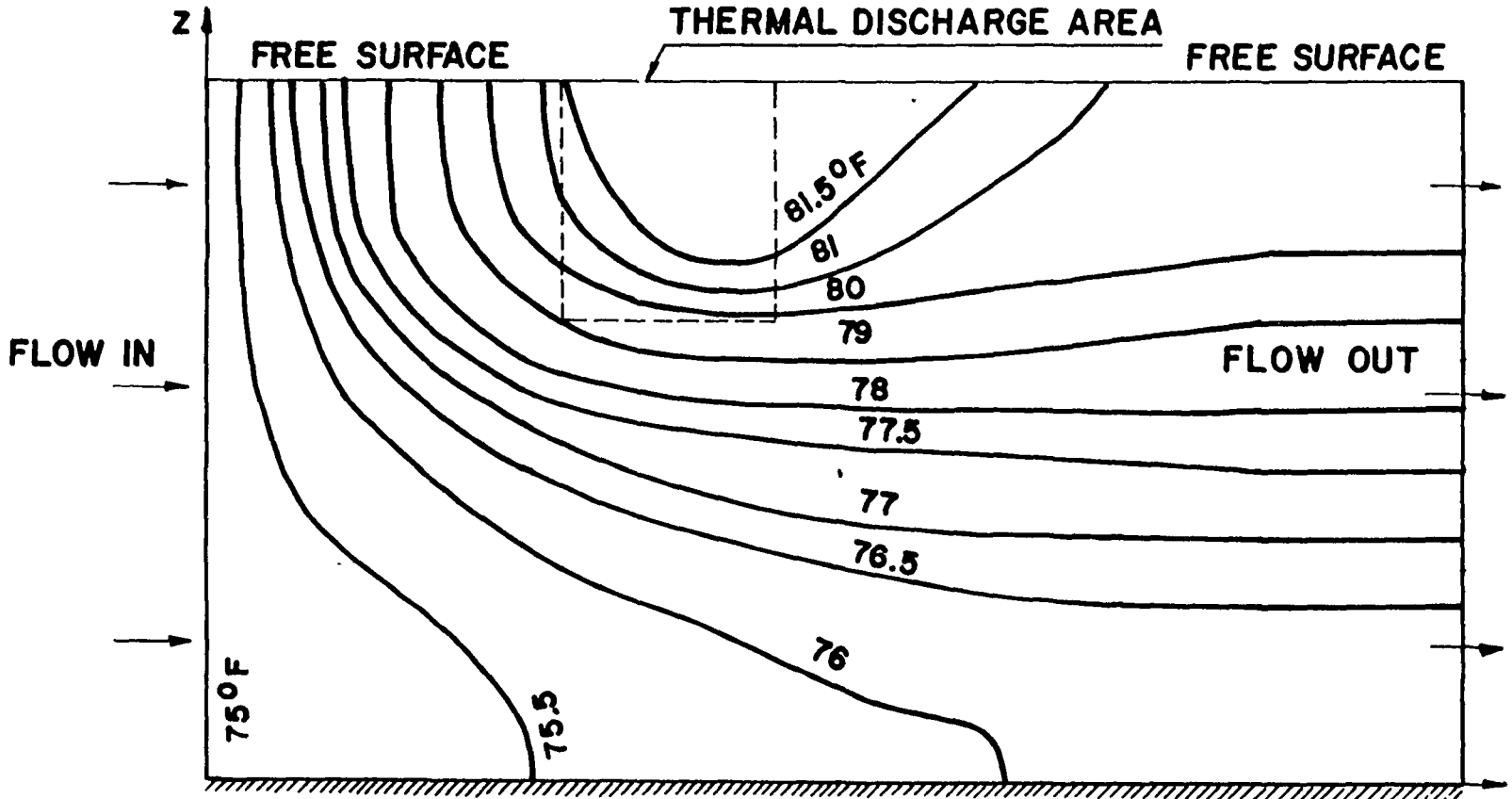

FIG 21. VERTICAL ISOTHERMS AT y = 100 FT. AND t = 500 SEC. IN THE WATER BODY SUBJECTED TO A BUOYANT JET

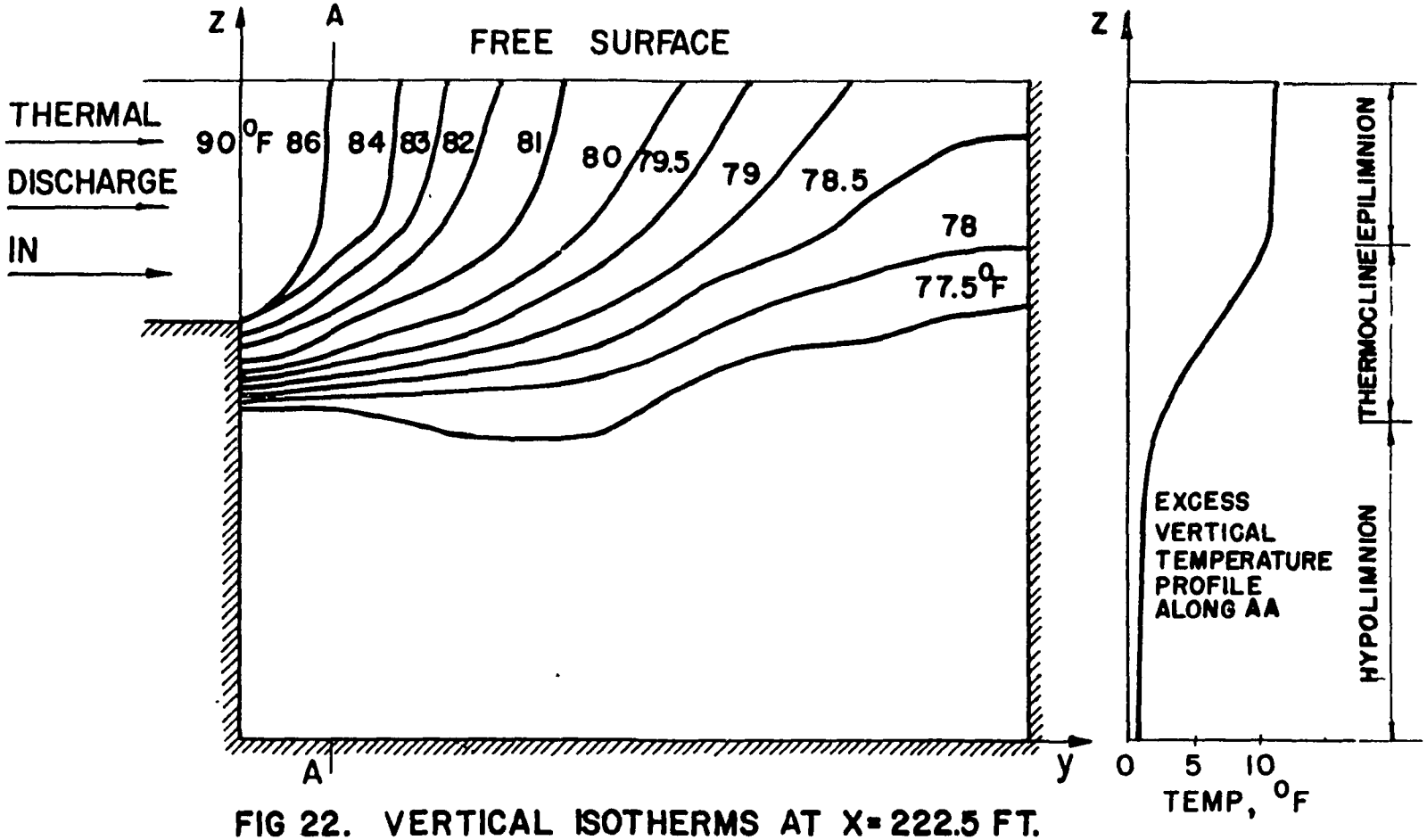

FIG 22. VERTICAL ISOTHERMS AT X = 222.5 FT. AND t = 500 SEC. IN THE WATER BODY SUBJECTED TO A BUOYANT JET